Optical Tomography and PhotoAcoustic Tomogrpahy

Simon R. Arridge[1] Joint work with :
B.Cox[3], A. Pulkkinen[2], T. Tarvainen[1,2]

[1]Department of Computer Science, University College London, UK
[2]Department of Physics and Mathematics, University of Eastern Finland, Finland
[3]Department of Medical Physics, University College London, UK

Inverse Problems Workshop
LMS, EPSRC Durham Symposium
Mathematical and Comptuational Aspects of Maxwell's Equations
11th-21st July 2016

Outline

1. Introduction
2. Modelling in Optical Tomography
3. PhotoAcoustics
4. Coupled Physics Imaging : Quantitative PhotoAcoustic Tomography
5. Summary
6. Acknowledgements

Outline

1. Introduction
2. Modelling in Optical Tomography
3. PhotoAcoustics
4. Coupled Physics Imaging : Quantitative PhotoAcoustic Tomography
5. Summary
6. Acknowledgements

Light propagation through tissue used for mammographic investigations (Cutler 1929)

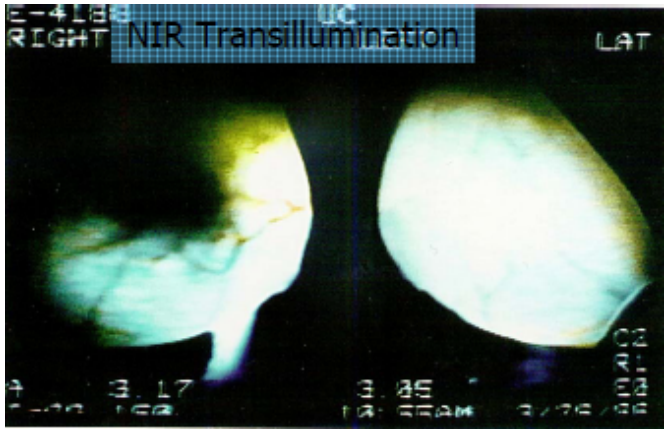

Light propagation through tissue used for mammographic investigations (Cutler 1929)

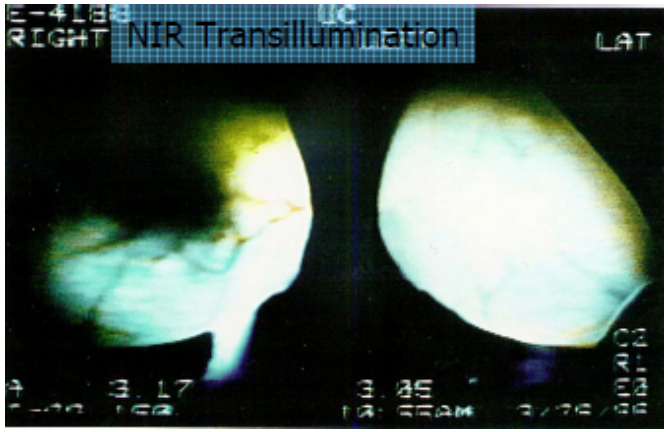

Jösis 1977, used optical radiation in the near-infrared band as a method for studying cerebral haemodynamics on the exposed cortex of a cat.

Noninvasive, Infrared Monitoring of Cerebral and Myocardial Oxygen Sufficiency and Circulatory Parameters

Abstract. *The relatively good transparency of biological materials in the near infrared region of the spectrum permits sufficient photon transmission through organs in situ for the monitoring of cellular events. Observations by infrared transillumination in the exposed heart and in the brain in cephalo without surgical intervention show that oxygen sufficiency for cytochrome a,a_3, function, changes in tissue blood volume, and the average hemoglobin-oxyhemoglobin equilibrium can be recorded effectively and in continuous fashion for research and clinical purposes. The copper atom associated with heme a_3 did not respond to anoxia and may be reduced under normoxic conditions, whereas the heme-a copper was at least partially reducible.*

Introduction

Near InfraRed Spectroscopy

- In Near Infrared Spectroscopy (NIRS), tissue is illuminated with selected wavelengths, and light that has travelled through the tissue between source and detector optodes is measured.

Introduction

Near InfraRed Spectroscopy

- In Near Infrared Spectroscopy (NIRS), tissue is illuminated with selected wavelengths, and light that has travelled through the tissue between source and detector optodes is measured.
- The change in chromophore concentration is assumed to be spread over the volume being measured. This leads to a partial-volume effect, and underestimation of the magnitude of localized changes.

Introduction

Near InfraRed Spectroscopy

- In Near Infrared Spectroscopy (NIRS), tissue is illuminated with selected wavelengths, and light that has travelled through the tissue between source and detector optodes is measured.
- The change in chromophore concentration is assumed to be spread over the volume being measured. This leads to a partial-volume effect, and underestimation of the magnitude of localized changes.
- From the attenuation of the light changes in the concentrations of chromophores such as oxygenated (HbO2) and deoxygenated heamoglobin (HbR), and cytochrome oxidase can be calculated.

Introduction

Near InfraRed Spectroscopy

- In Near Infrared Spectroscopy (NIRS), tissue is illuminated with selected wavelengths, and light that has travelled through the tissue between source and detector optodes is measured.
- The change in chromophore concentration is assumed to be spread over the volume being measured. This leads to a partial-volume effect, and underestimation of the magnitude of localized changes.
- From the attenuation of the light changes in the concentrations of chromophores such as oxygenated (HbO2) and deoxygenated heamoglobin (HbR), and cytochrome oxidase can be calculated.
- NIRS is widely used to refer to monitoring of haemodynamic processes in tissues such as muscle and breast, and the brain of both adults and infants.

Introduction

functional Near Infra Red Spectroscopy

Functional Near Infrared Spectroscopy (fNIRS) refers to the application of NIRS to the haemodynamic *response* to an external stimulus; this is a direct analogy to the term *Functional Magnetic Resonance Imaging* (fMRI) as distinguished from strutural or “static” MRI. Thus fNIRS is a *dynamic* modality (compare fMRI).

Introduction

functional Near Infra Red Spectroscopy

Functional Near Infrared Spectroscopy (fNIRS) refers to the application of NIRS to the haemodynamic *response* to an external stimulus; this is a direct analogy to the term *Functional Magnetic Resonance Imaging* (fMRI) as distinguished from strutural or “static” MRI. Thus fNIRS is a *dynamic* modality (compare fMRI).

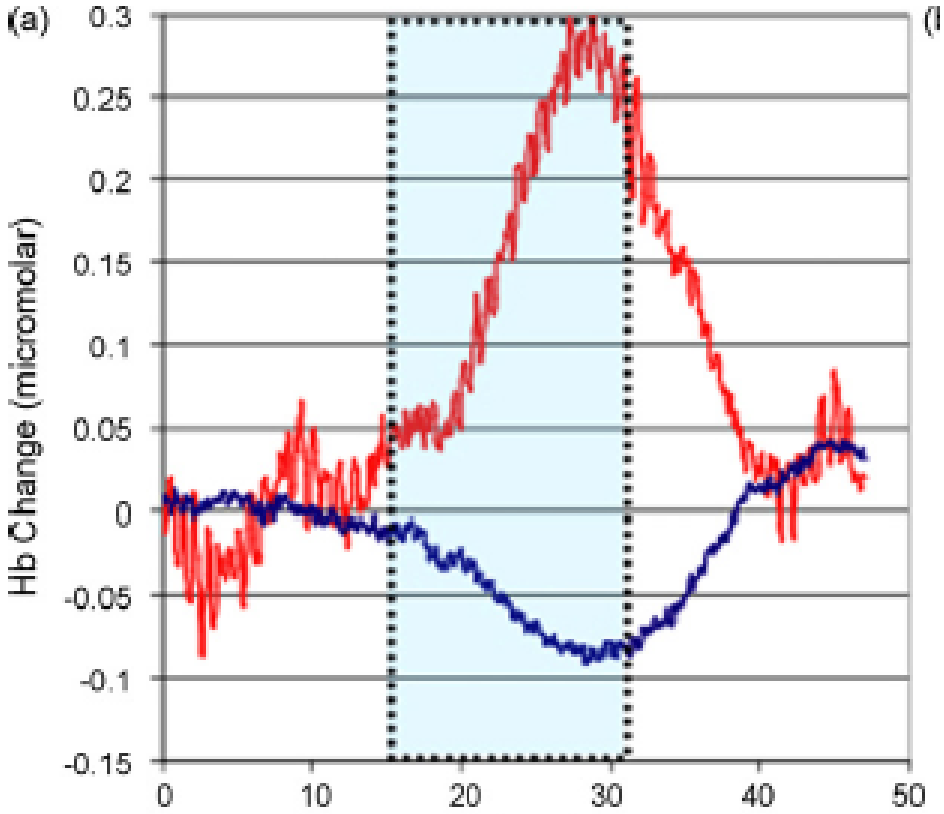

- OT is faster than fNIRS
- OT gives a *spectral* contrast

figure taken from
S. Lloyd-Fox, Neuroscience and BioBehavioral Reviews 2009

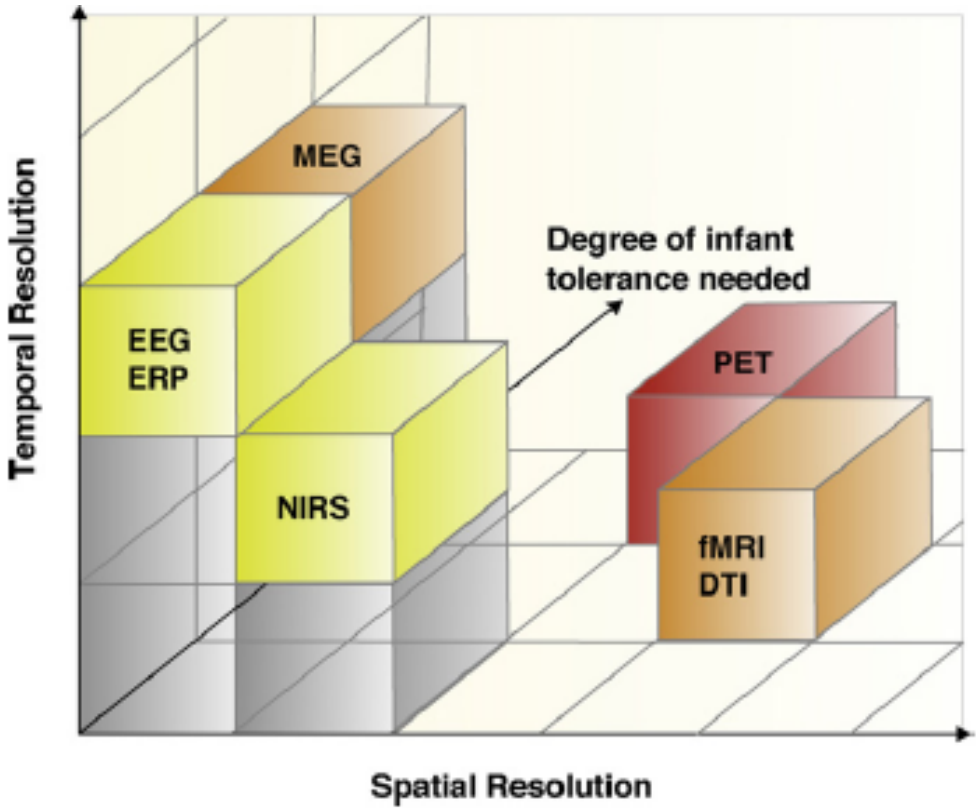

Fig. 2. This figure shows the spatial and temporal resolution of NIRS compared with other infant functional neuroimaging methods. It also illustrates the relative degree of tolerance needed from the infant for each method, ranging from yellow (low) to red (high). EEG, electroencephalography; ERP, event-related potential; MEG, magnetoencephalography; NIRS, near infrared spectroscopy; fMRI, functional magnetic resonance imaging; DTI, diffusion tensor imaging; PET, positron emission tomography. (This figure was inspired by Walsh and Cowey, 2000.) (For interpretation of the references to color in this figure legend, the reader is referred to the web version of the article.)

Optical Tomography

Neonatal imaging

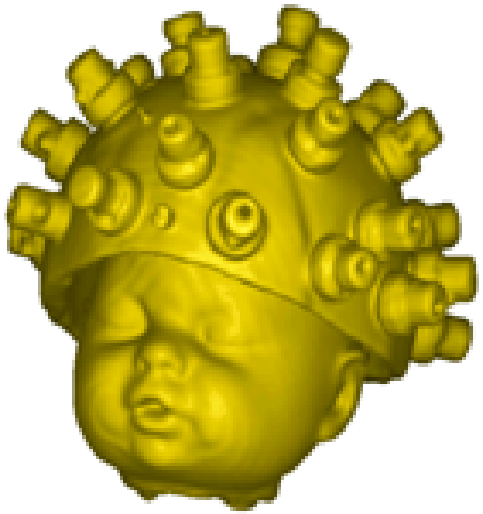

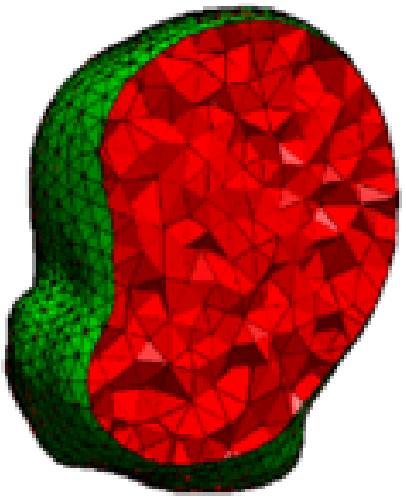

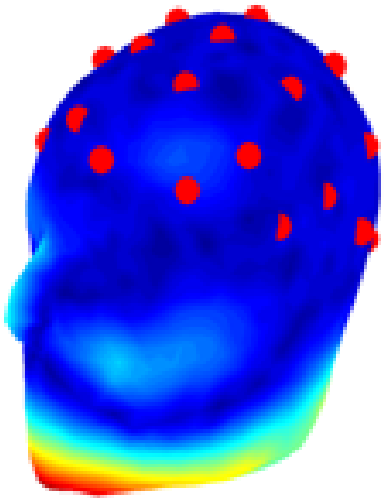

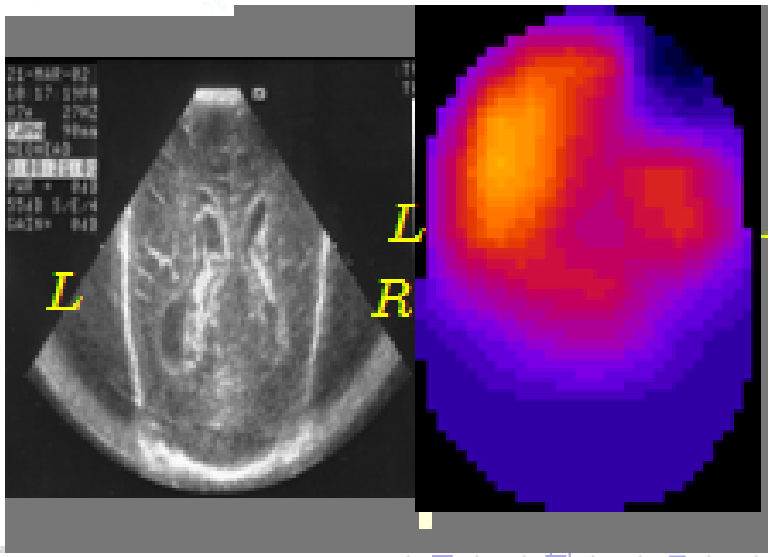

Optical Tomography

Neonatal imaging

Figure 1. A fibre holder helmet on the head of an infant during an imaging scan

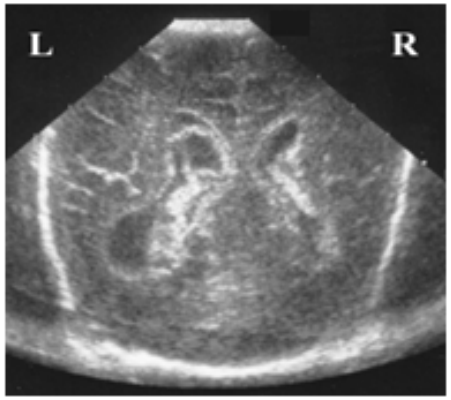

Figure 2. Ultrasound image of infant with haemorrhage in left ventricle.

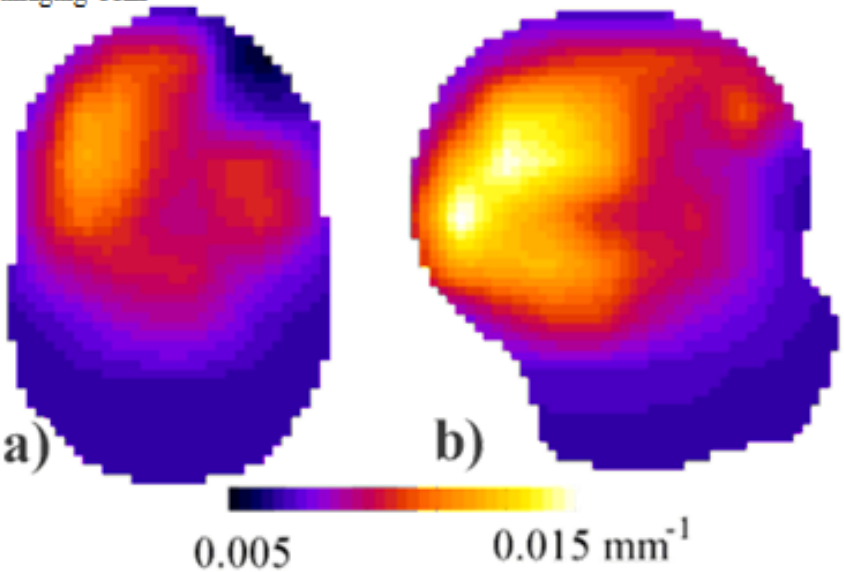

Figure 3. Absorption images of infant brain with left-side haemorrhage: a) Coronal and b) sagittal views.

Outline

1. Introduction
2. Modelling in Optical Tomography
3. PhotoAcoustics
4. Coupled Physics Imaging : Quantitative PhotoAcoustic Tomography
5. Summary
6. Acknowledgements

The Radiative Transfer Equation (RTE) is a natural description of light considered as photons. It represents a balance equation where photons in a constant refractive index medium, in the absence of scattering, are propagated along rays $\boldsymbol{l} := \boldsymbol{r}_0 + l\hat{\boldsymbol{s}}$

$$\hat{\boldsymbol{s}} \cdot \nabla\phi + \mu_a\phi = 0 \quad \equiv \quad \mathcal{T}_{\mu_a}\phi = 0 \tag{1}$$

whose solution

$$\phi = \phi_0 \exp\left[-\int_{\boldsymbol{l}} \mu_a(\boldsymbol{r}_0 + l\hat{\boldsymbol{s}})\mathrm{d}l\right] \tag{2}$$

is the basis for the definition of the *Ray Transform*

$$g_{\hat{\boldsymbol{s}}}(p) := -\ln\left[\frac{\phi}{\phi_0}\right] = \int_{-\infty}^{\infty} \mu_a(p\hat{\boldsymbol{s}}_\perp + l\hat{\boldsymbol{s}})\mathrm{d}l \quad \equiv \quad g_{\hat{\boldsymbol{s}}} = \mathcal{R}_{\hat{\boldsymbol{s}}}\mu_a \tag{3}$$

In the presence of scattering, and with source terms q, eq.(1) becomes

$$\begin{aligned}(\hat{\boldsymbol{s}}\cdot\nabla+\mu_{\mathrm{a}}(\boldsymbol{r})+\mu_{\mathrm{s}}(\boldsymbol{r}))\,\phi(\boldsymbol{r},\hat{\boldsymbol{s}}) &= \mu_{\mathrm{s}}\int_{S^{n-1}}\Theta(\hat{\boldsymbol{s}},\hat{\boldsymbol{s}}')\phi(\boldsymbol{r},\hat{\boldsymbol{s}}')d\hat{\boldsymbol{s}}'+q(\boldsymbol{r},\hat{\boldsymbol{s}})\\ \equiv \underbrace{[\mathcal{T}_{\mu_{\mathrm{tr}}}-\mu_{\mathrm{s}}\mathcal{S}]}_{\mathcal{L}}\phi &= q \end{aligned} \tag{4}$$

$\mu_{\mathrm{tr}}=\mu_{\mathrm{s}}+\mu_{\mathrm{a}}$ is the attenuation coefficent
$\mathcal{S}$ is the scattering operator, (local, non propagating).
Method of successive approximation (Sobolev 1963) :

$$\phi=\left[\mathcal{T}_{\mu_{\mathrm{tr}}}^{-1}+\mathcal{T}_{\mu_{\mathrm{tr}}}^{-1}\mu_{\mathrm{s}}\mathcal{S}\mathcal{T}_{\mu_{\mathrm{tr}}}^{-1}+\ldots\left(\mathcal{T}_{\mu_{\mathrm{tr}}}^{-1}\mu_{\mathrm{s}}\mathcal{S}\right)^{k}\mathcal{T}_{\mu_{\mathrm{tr}}}^{-1}\ldots\right]q \tag{5}$$

The first term may be found from the Ray Transform, giving an alternative equation for the *collided flux*

$$[\mathcal{T}_{\mu_{\mathrm{tr}}}-\mu_{\mathrm{s}}\mathcal{S}]\,\phi_{\mathrm{collided}}=\mu_{\mathrm{s}}\mathcal{S}\underbrace{\mathcal{T}_{\mu_{\mathrm{tr}}}^{-1}q}_{\text{uncollided}} \tag{6}$$

Modelling in Optical Tomography

RTE solutions

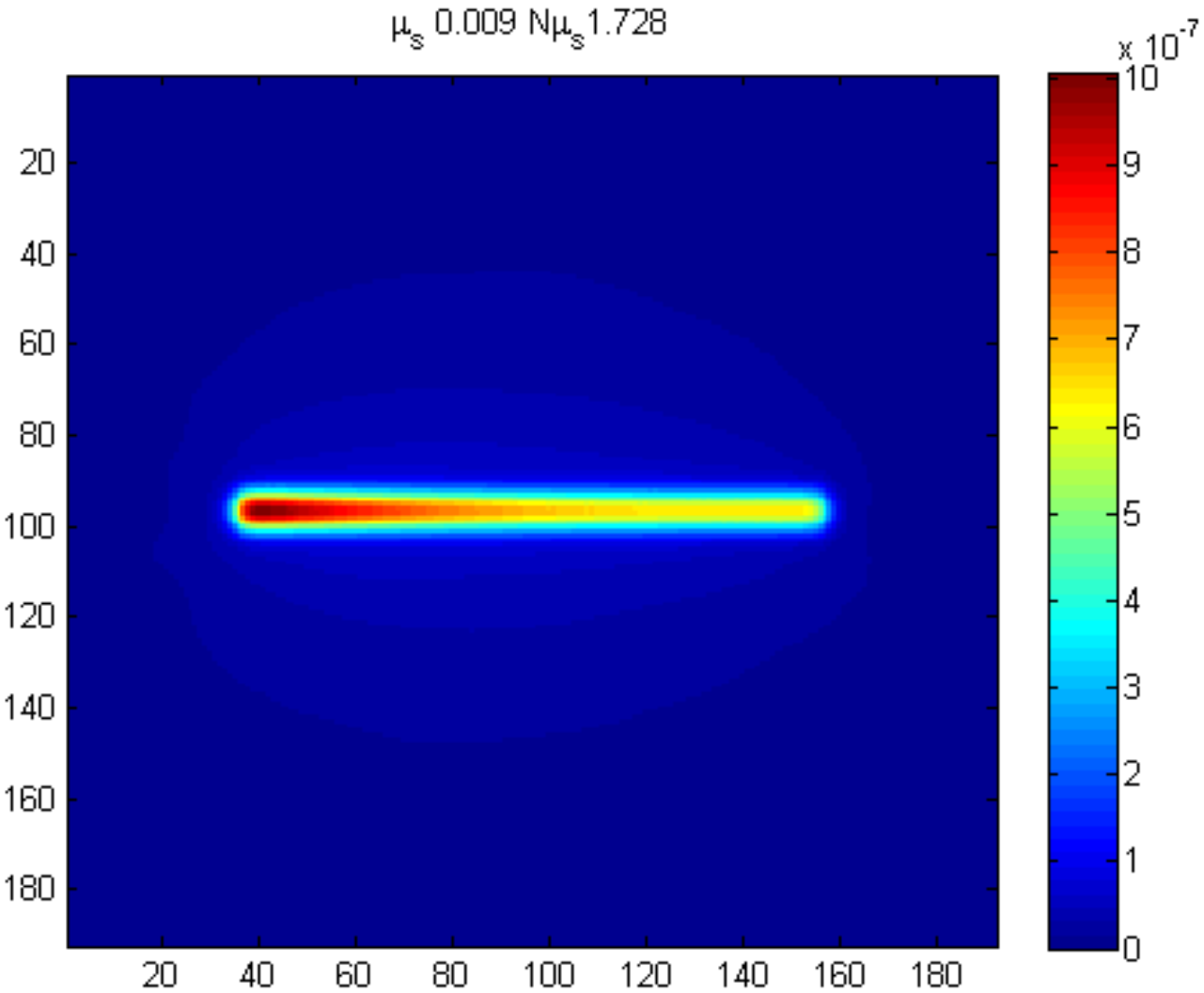

Modelling in Optical Tomography

RTE solutions

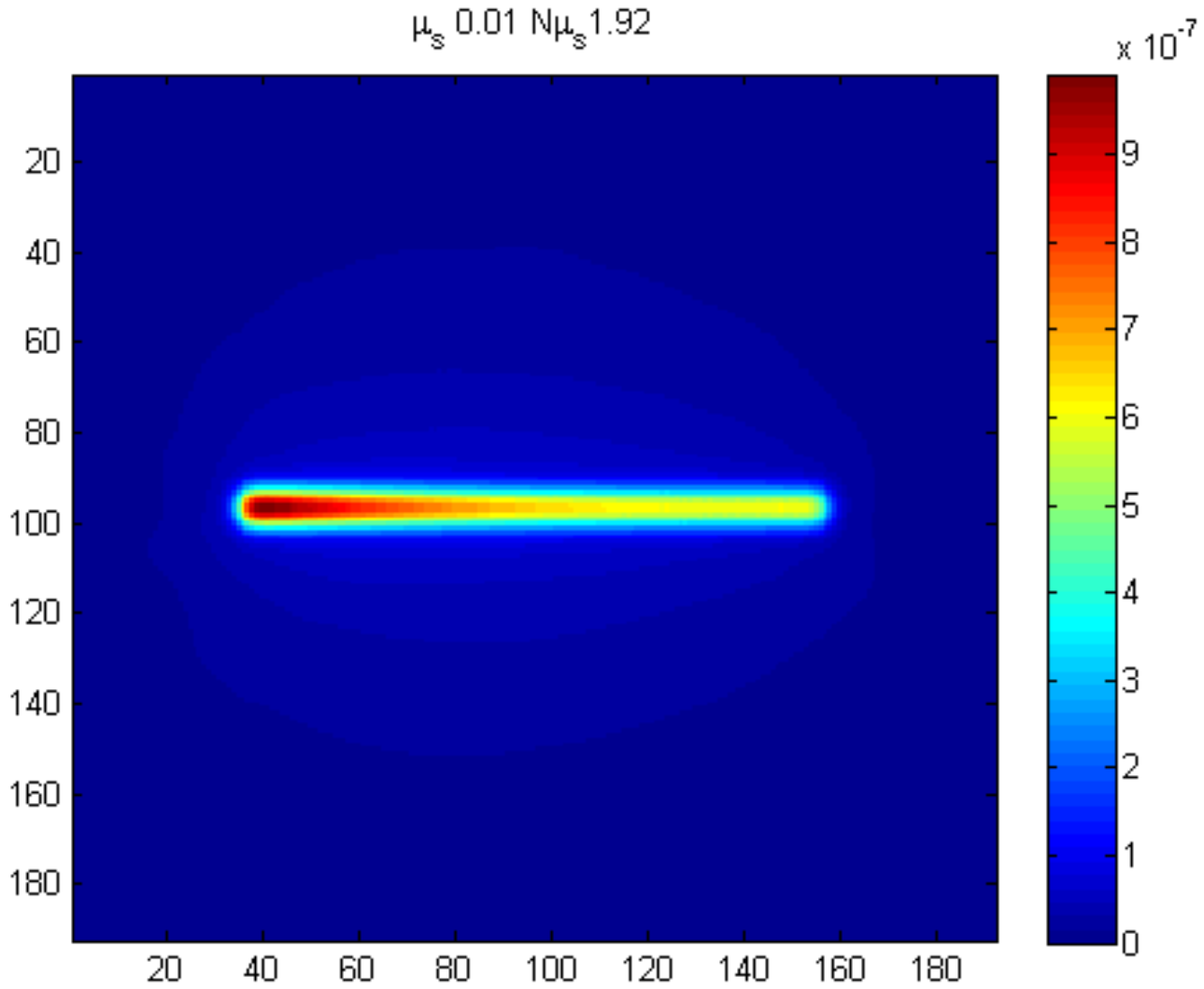

Modelling in Optical Tomography

RTE solutions

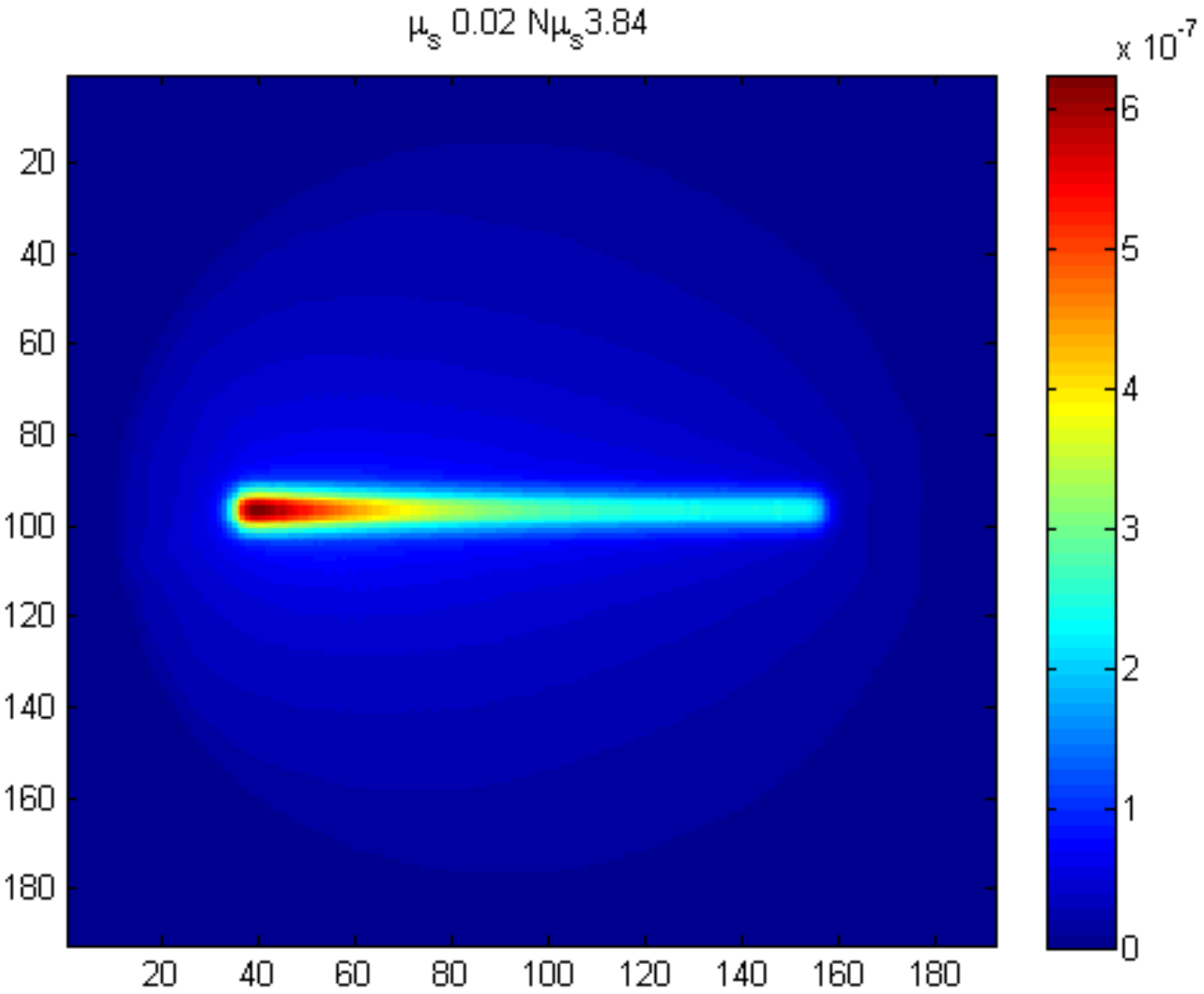

Modelling in Optical Tomography

RTE solutions

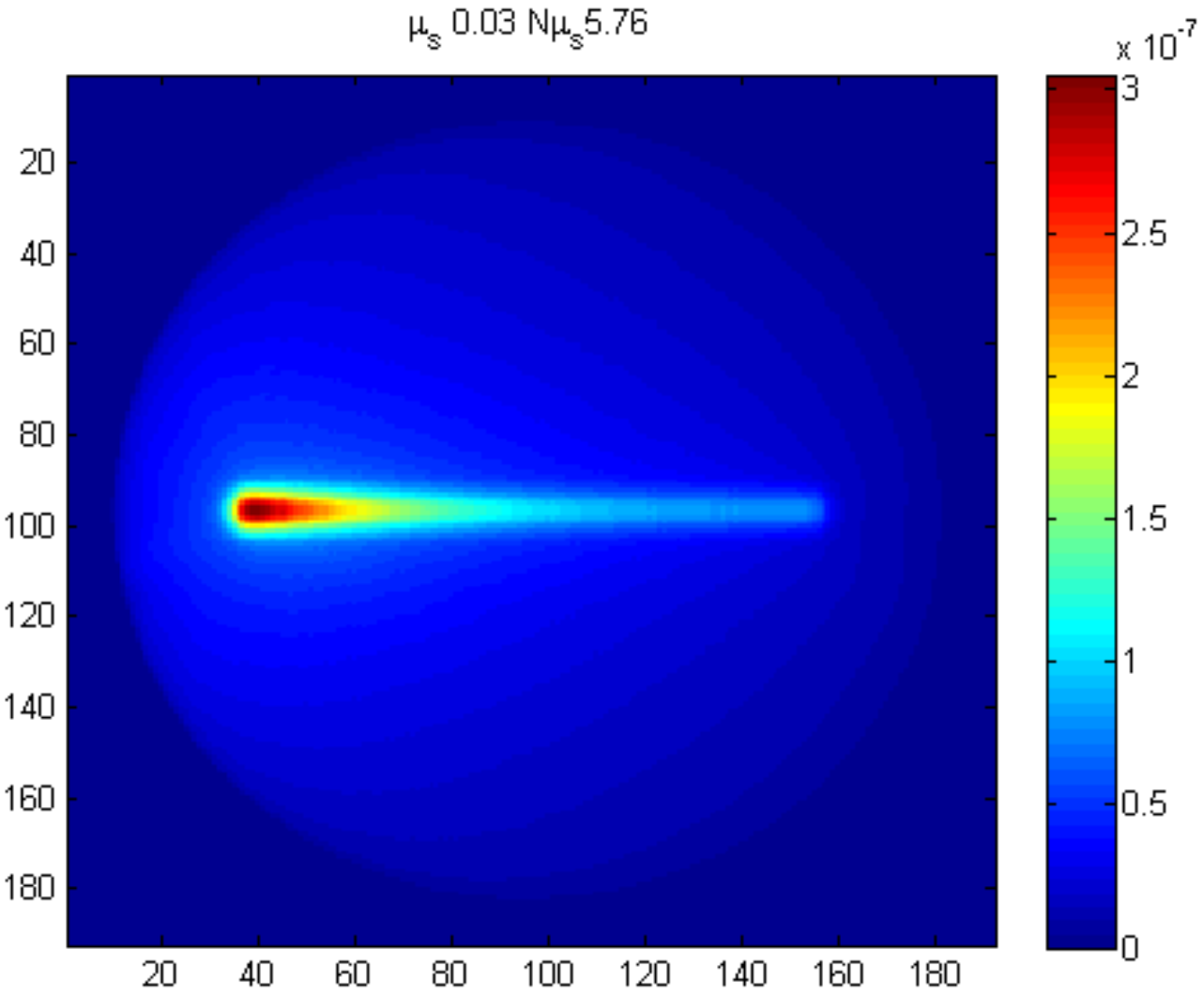

Modelling in Optical Tomography

RTE solutions

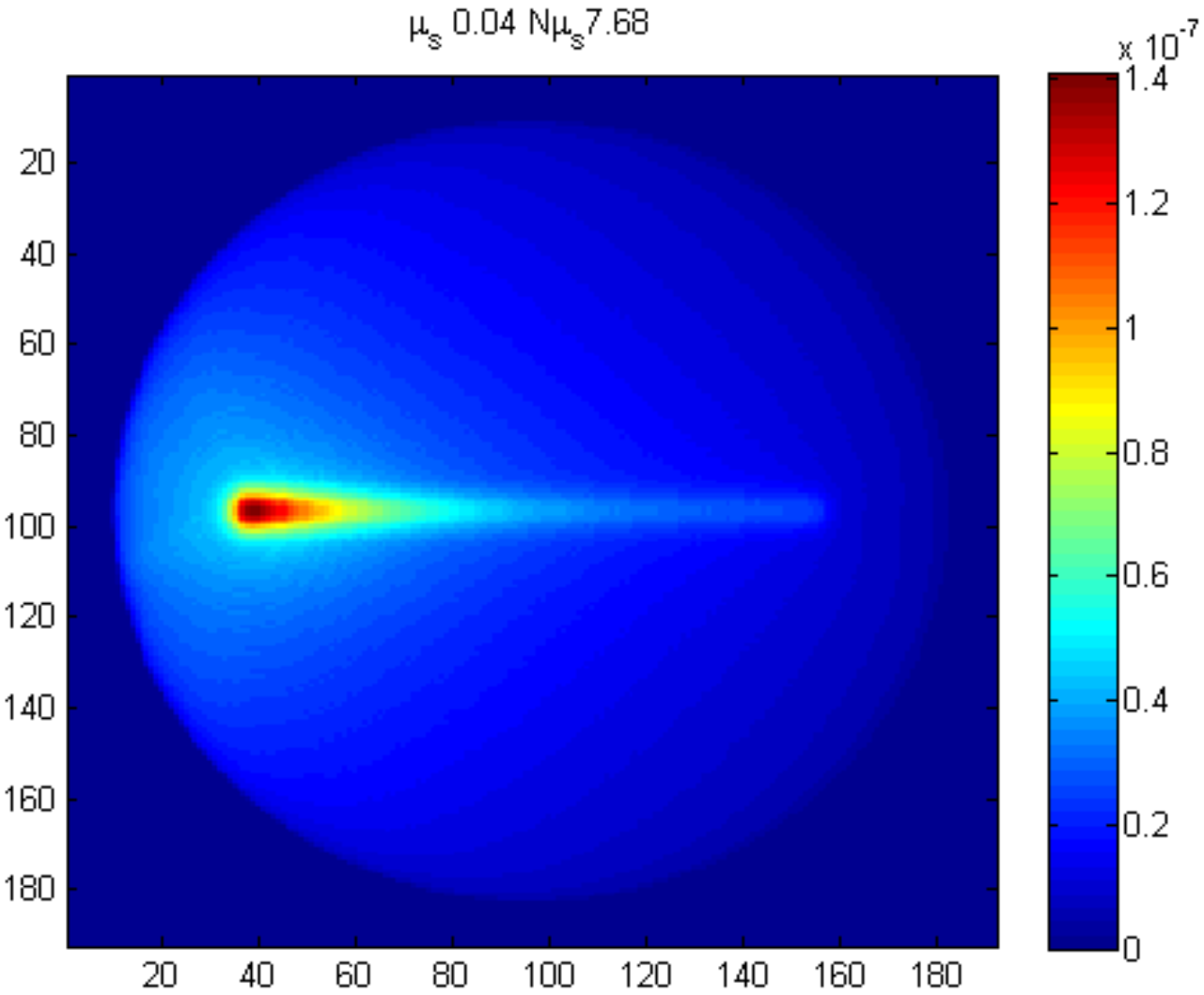

Modelling in Optical Tomography

RTE solutions

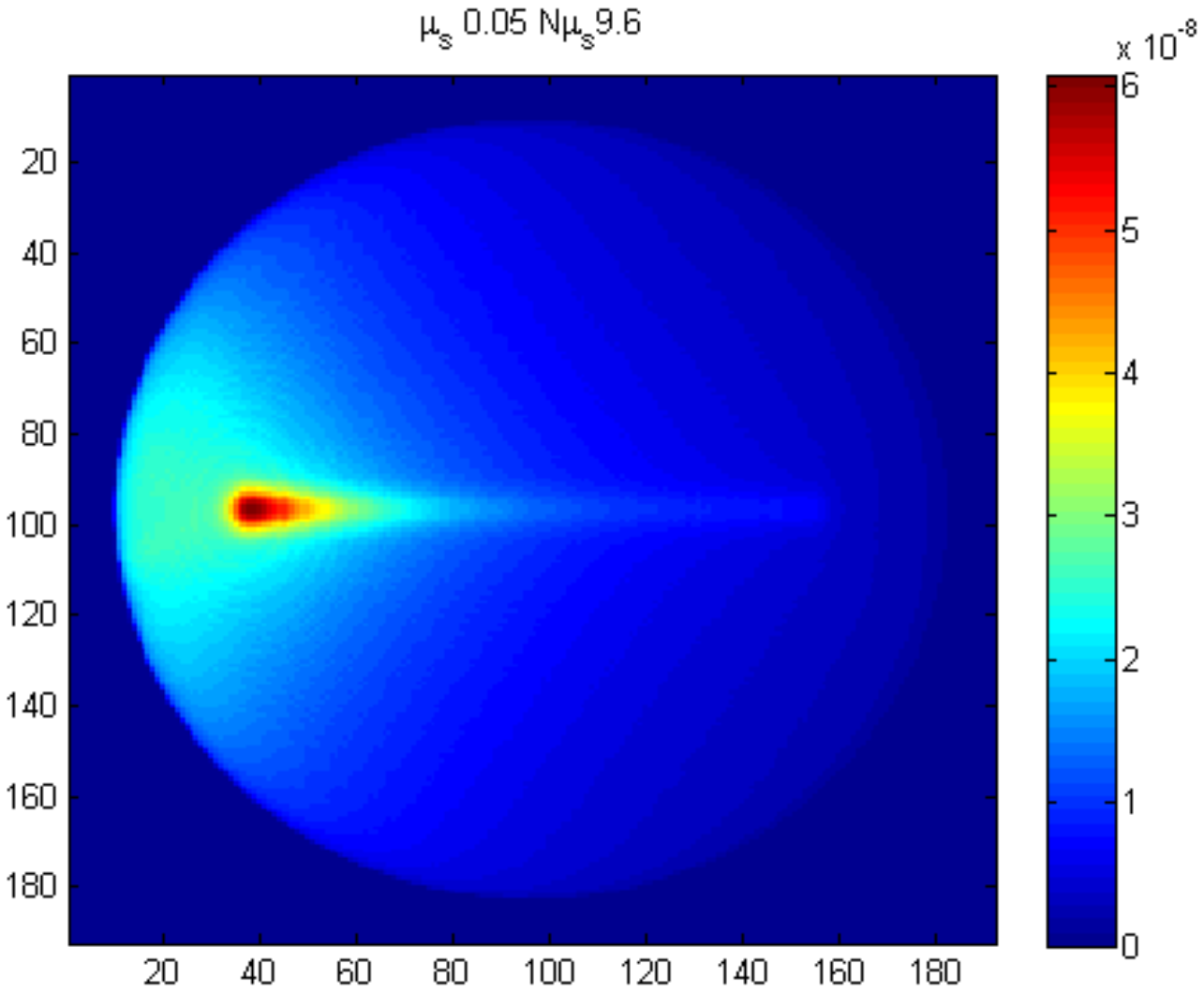

Modelling in Optical Tomography

RTE solutions

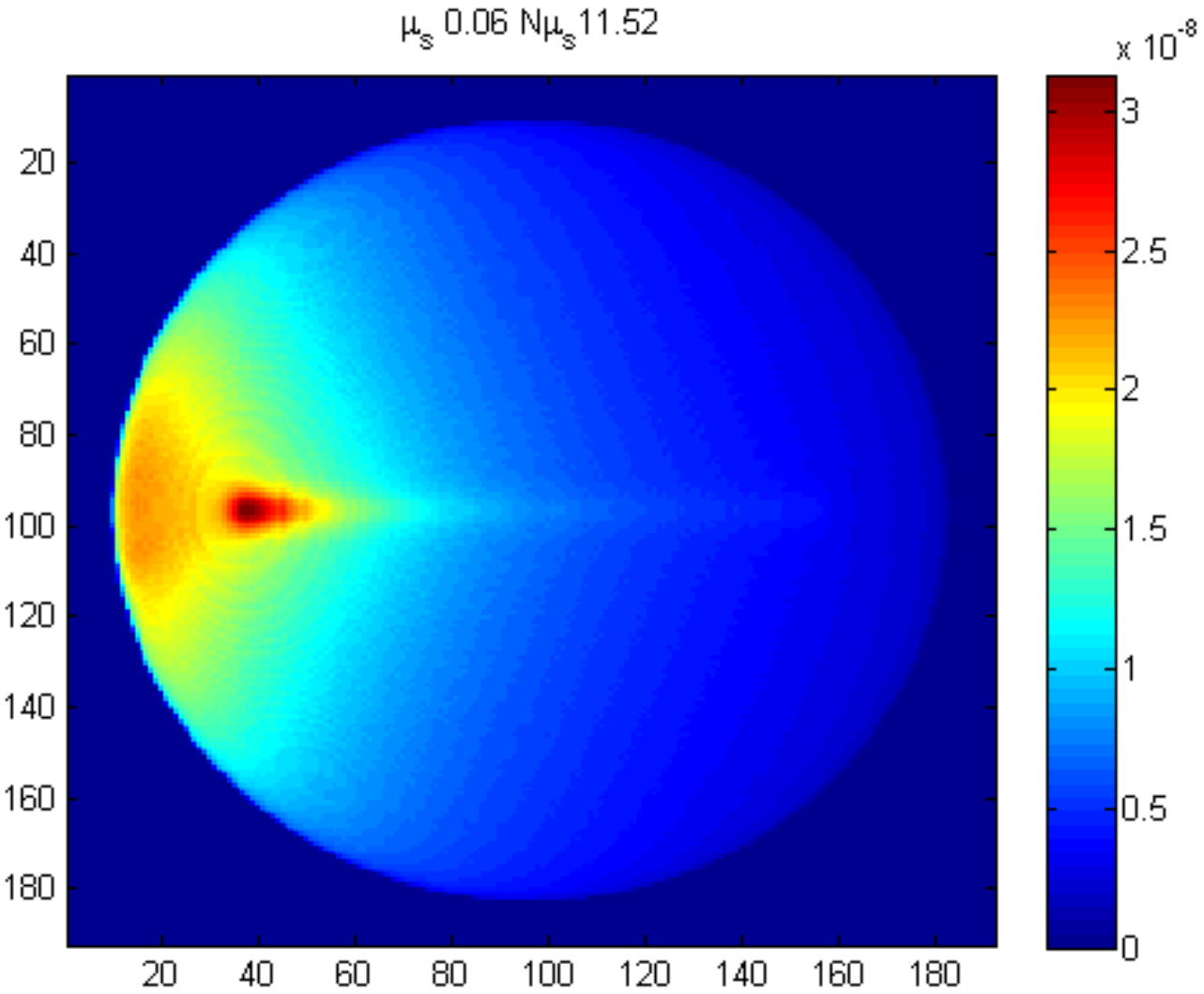

Modelling in Optical Tomography

RTE solutions

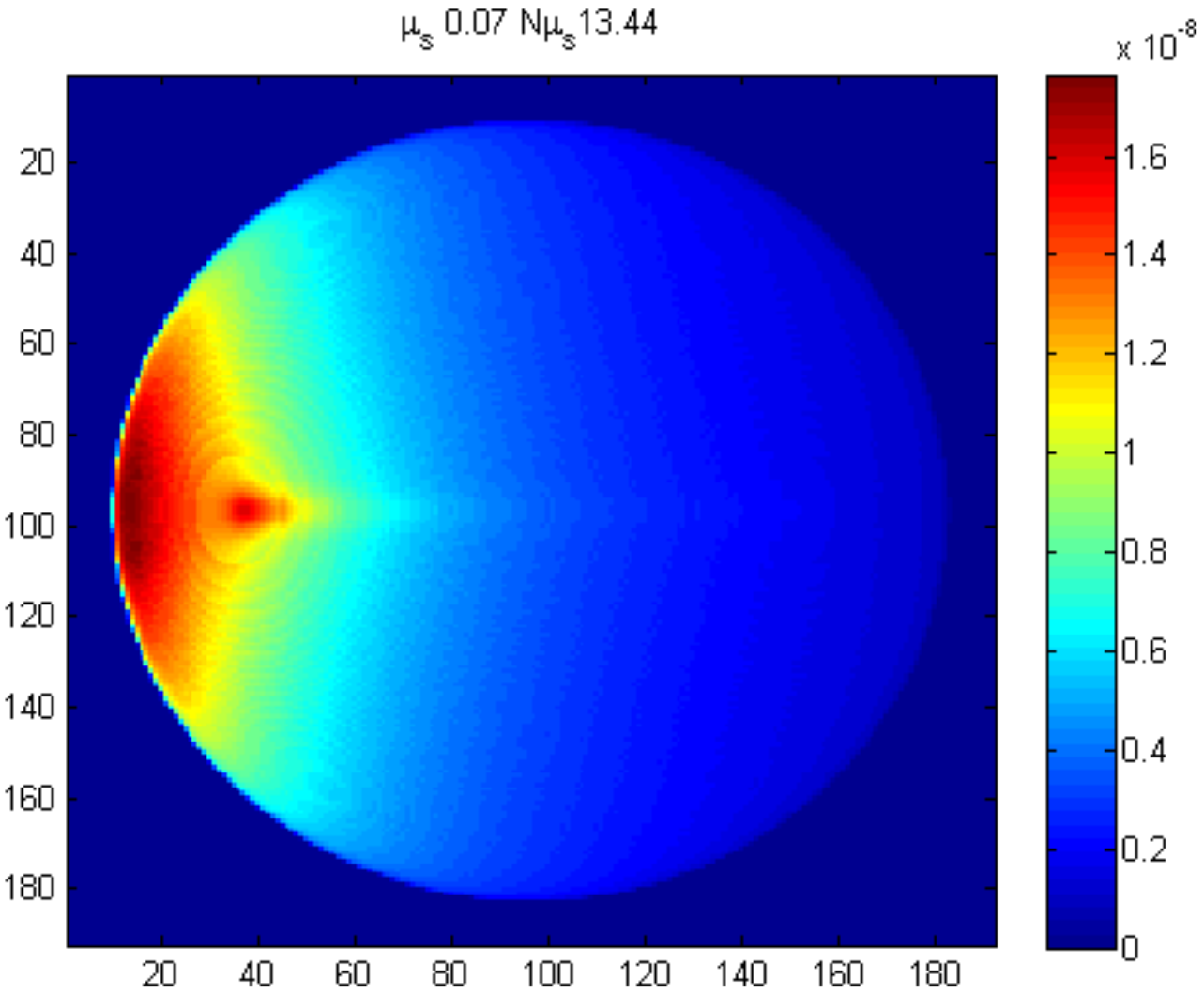

Modelling in Optical Tomography

RTE solutions

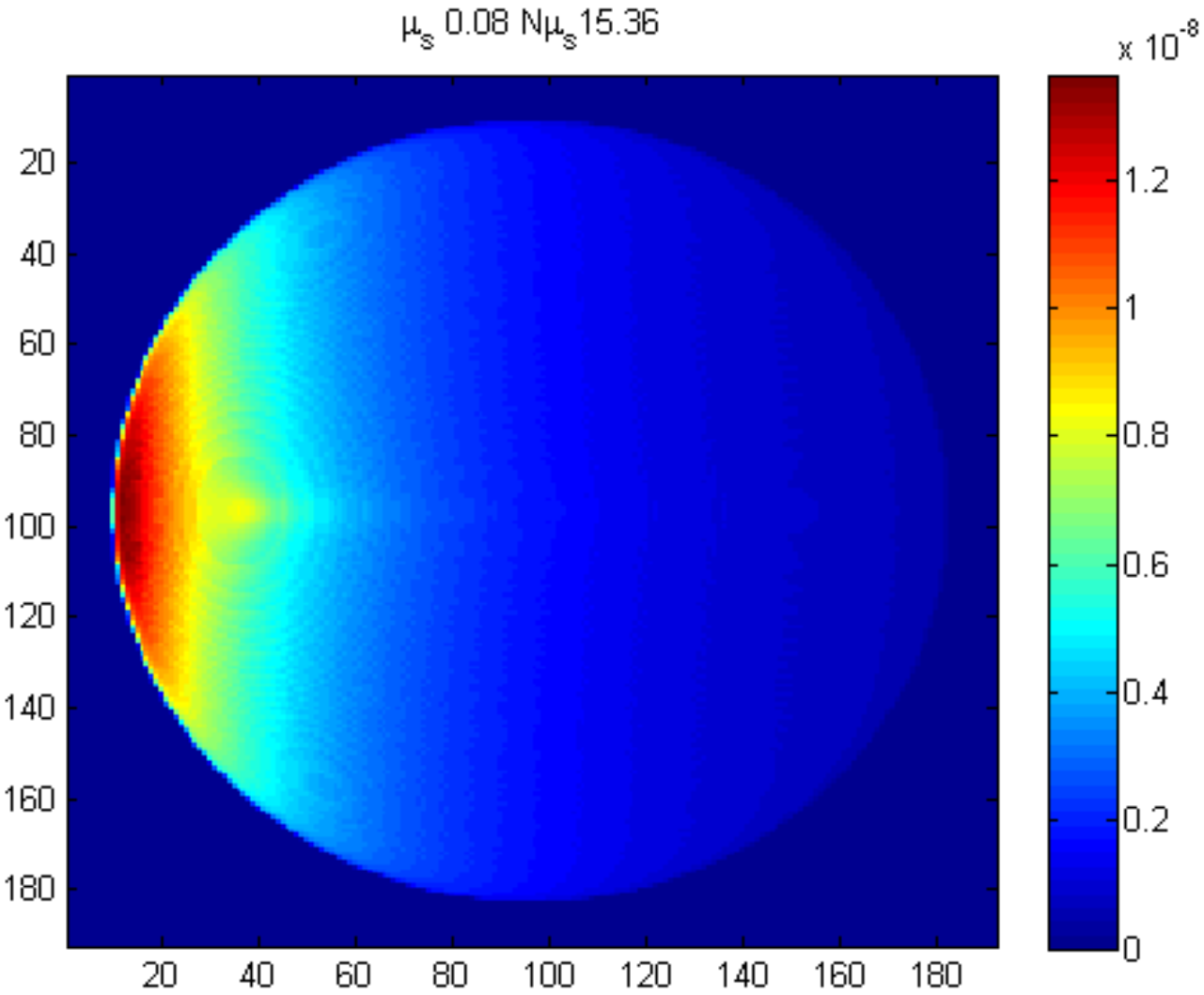

In the Diffusion pproximation (DA), the radiance is approximated by first order spherical harmonics only ($\hat{\boldsymbol{s}} \equiv [Y_{1,-1}, Y_{1,0}, Y_{1,1}]$), giving

$$\phi(\boldsymbol{r}, \hat{\boldsymbol{s}}) \approx \frac{1}{4\pi}\Phi(\boldsymbol{r}) + \frac{3}{4\pi}\hat{\boldsymbol{s}} \cdot J(\boldsymbol{r}) \tag{7}$$

where $\Phi(\boldsymbol{r})$ and $J(\boldsymbol{r})$ are the photon density and current defined as

$$\Phi(\boldsymbol{r}) = \int_{S^{n-1}} \phi(\boldsymbol{r}, \hat{\boldsymbol{s}}) \mathrm{d}\hat{\boldsymbol{s}} \tag{8}$$

$$J(\boldsymbol{r}) = \int_{S^{n-1}} \hat{\boldsymbol{s}}\phi(\boldsymbol{r}, \hat{\boldsymbol{s}}) \mathrm{d}\hat{\boldsymbol{s}}. \tag{9}$$

Inserting the approximation (7) into equation (4) results in a second order PDE in the photon density

$$-\nabla \cdot \kappa \nabla \Phi(\boldsymbol{r}) + \mu_{\mathrm{a}}\Phi(\boldsymbol{r}) = q_0(\boldsymbol{r}) \quad \equiv \mathcal{D}\Phi = q_0 \ , \tag{10}$$

with $\kappa = \frac{1}{\mu_{\mathrm{a}} + (1-g)\mu_{\mathrm{s}})}$. Equation(10) and its associated frequency and time domain versions, including the Telegraph Equation, are the most commonly used in DOI.

Non-linear reconstruction

$x \equiv \{\mu_a, \kappa\}$ or $x \equiv \{\mu_a, \mu_s'\}$ and

$$A_i' \begin{pmatrix} \mu_a^\delta \\ \kappa^\delta \end{pmatrix} = -\int_\Omega \begin{pmatrix} U_i^* U_i \\ \nabla U_i^* \cdot \nabla U_i \end{pmatrix} \cdot \begin{pmatrix} \mu_a^\delta \\ \kappa^\delta \end{pmatrix}$$

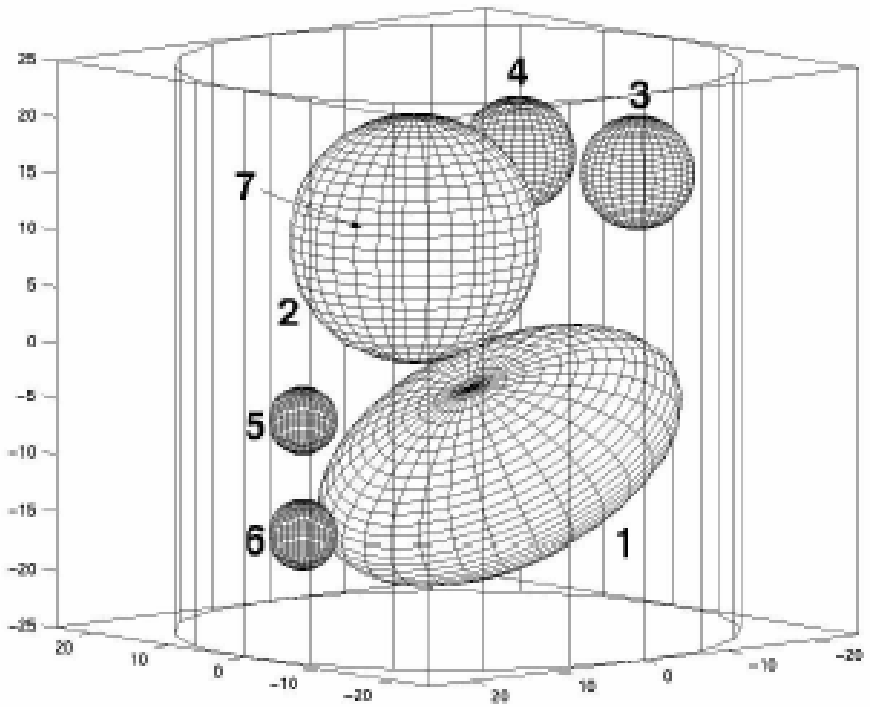

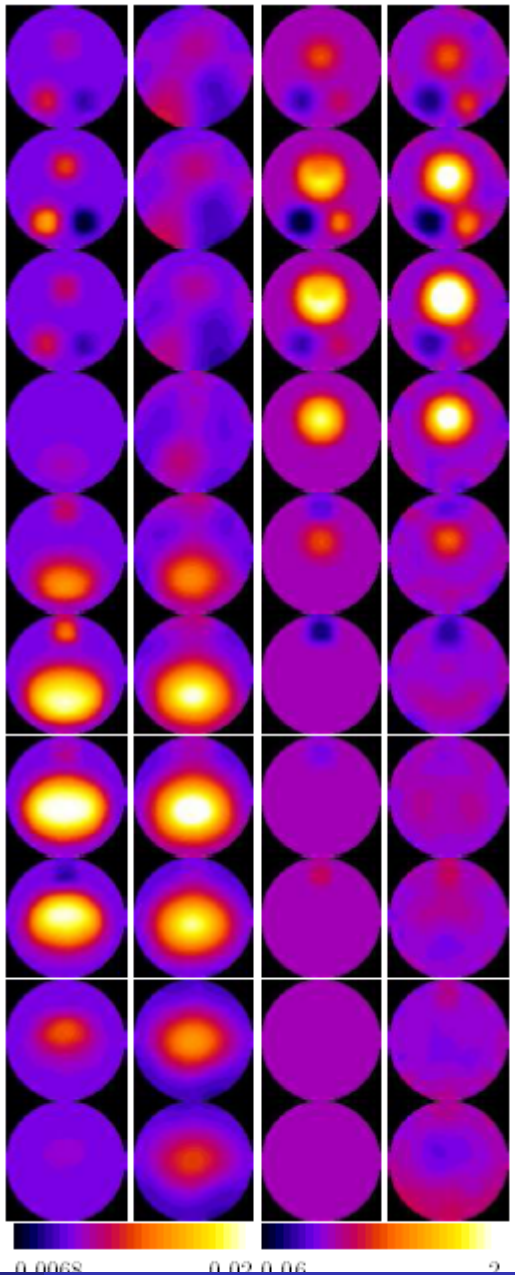

Outline

1. Introduction
2. Modelling in Optical Tomography
3. PhotoAcoustics
4. Coupled Physics Imaging : Quantitative PhotoAcoustic Tomography
5. Summary
6. Acknowledgements

The Early Years…

1. **1880** Alexander Graham Bell observes photoacoustic effect
2. **1960** Invention of the laser by Theodore Maiman
3. **1995** First photoacoustic image of a tissue phantom (R. Kruger)
4. **1999** First *in vivo* image (A. Oraevsky)
5. **2003** *In vivo* non invasive image of the mouse brain (L. Wang)

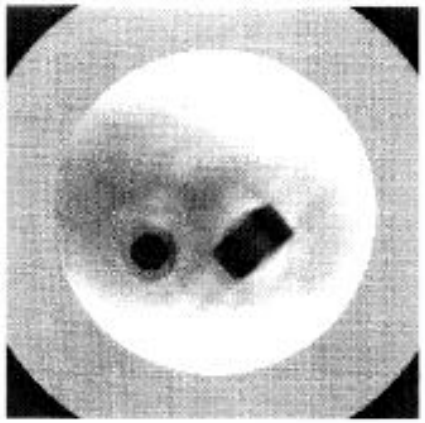

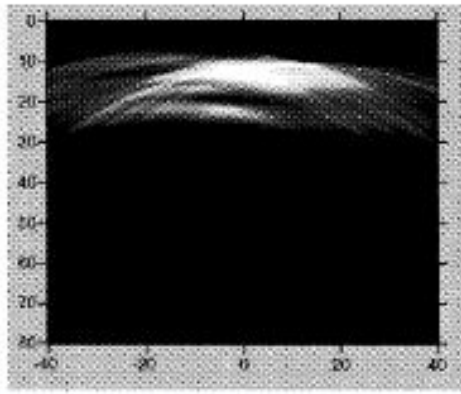

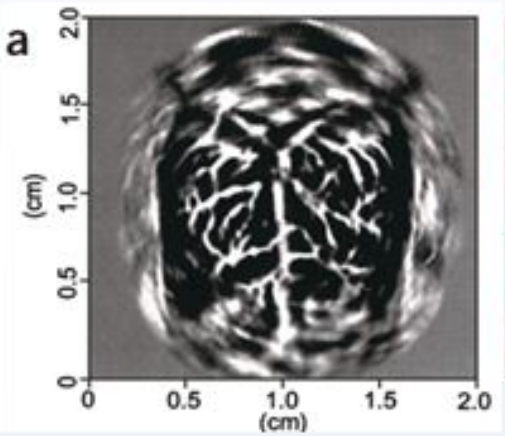

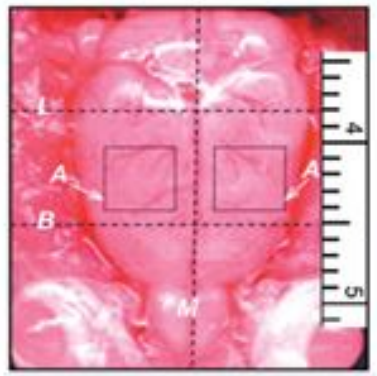

PhotoAcoustic Tomography

Motivation

- Optical Imaging : Pros
  - High intrinsic contrast based upon optical absorption and scattering
  - Spectroscopic specificity – chemical information
  - Functional imaging of physiological parameters – blood oxygenation
- Optical Imaging : Cons
  - Imaging depth/spatial resolution limited by strong optical scattering
- Ultrasound Imaging : Pros
  - Images of soft tissue anatomy
  - High spatial resolution: scalable with depth 100's $\mu m - - \sim mm$
  - Large penetration depth: $\sim 10cm$
  - Physiological information via measurement of blood flow
- Ultrasound Imaging : Cons
  - Weak contrast provided by certain important targets – e.g. the microvasculature
  - Limited specificity: weak sensitivity to chemical differences

PhotoAcoustic Tomography

PhotoAcoustic Signal Generation

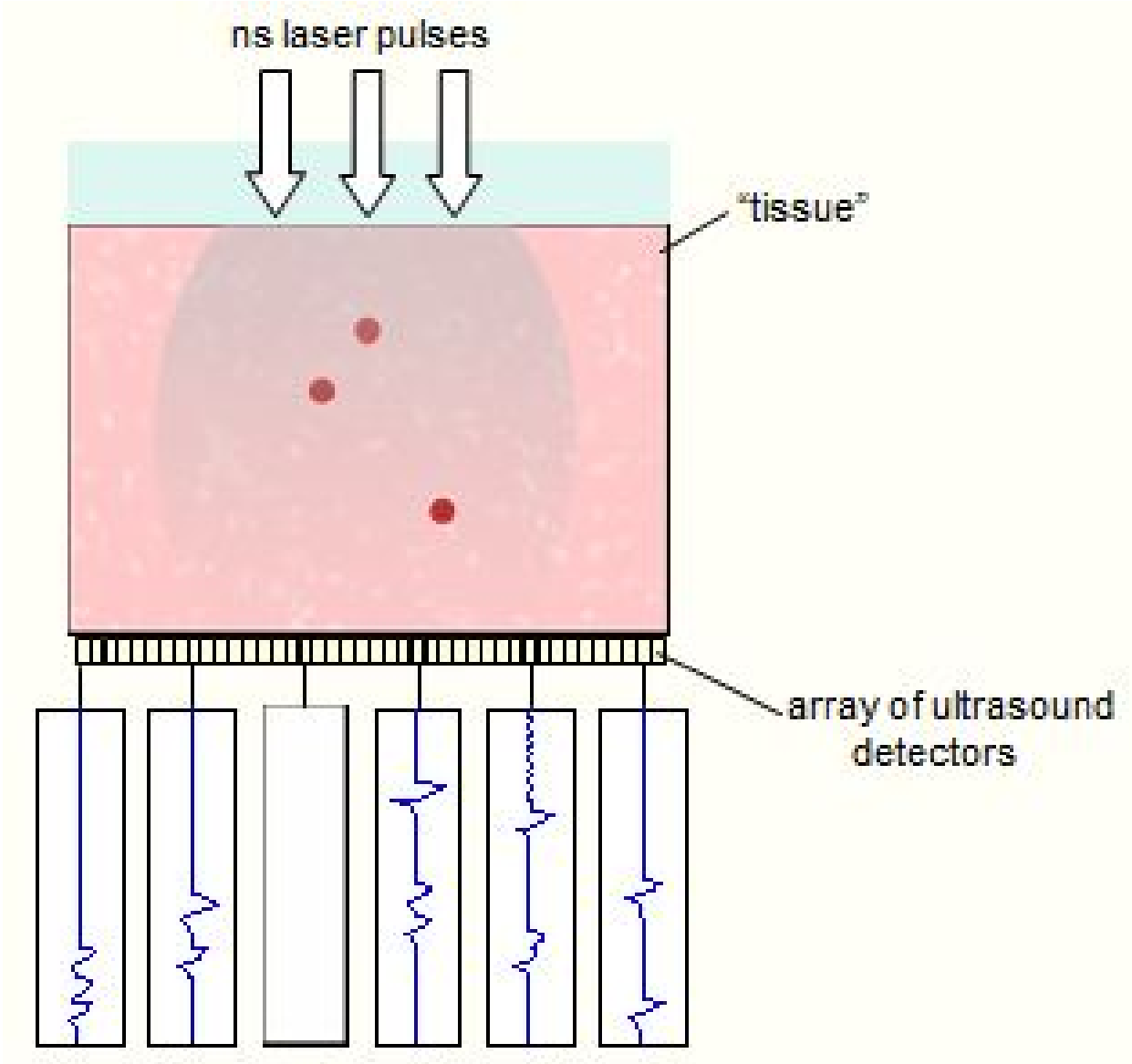

PhotoAcoustic Tomography

PhotoAcoustic Spherical BackProjection

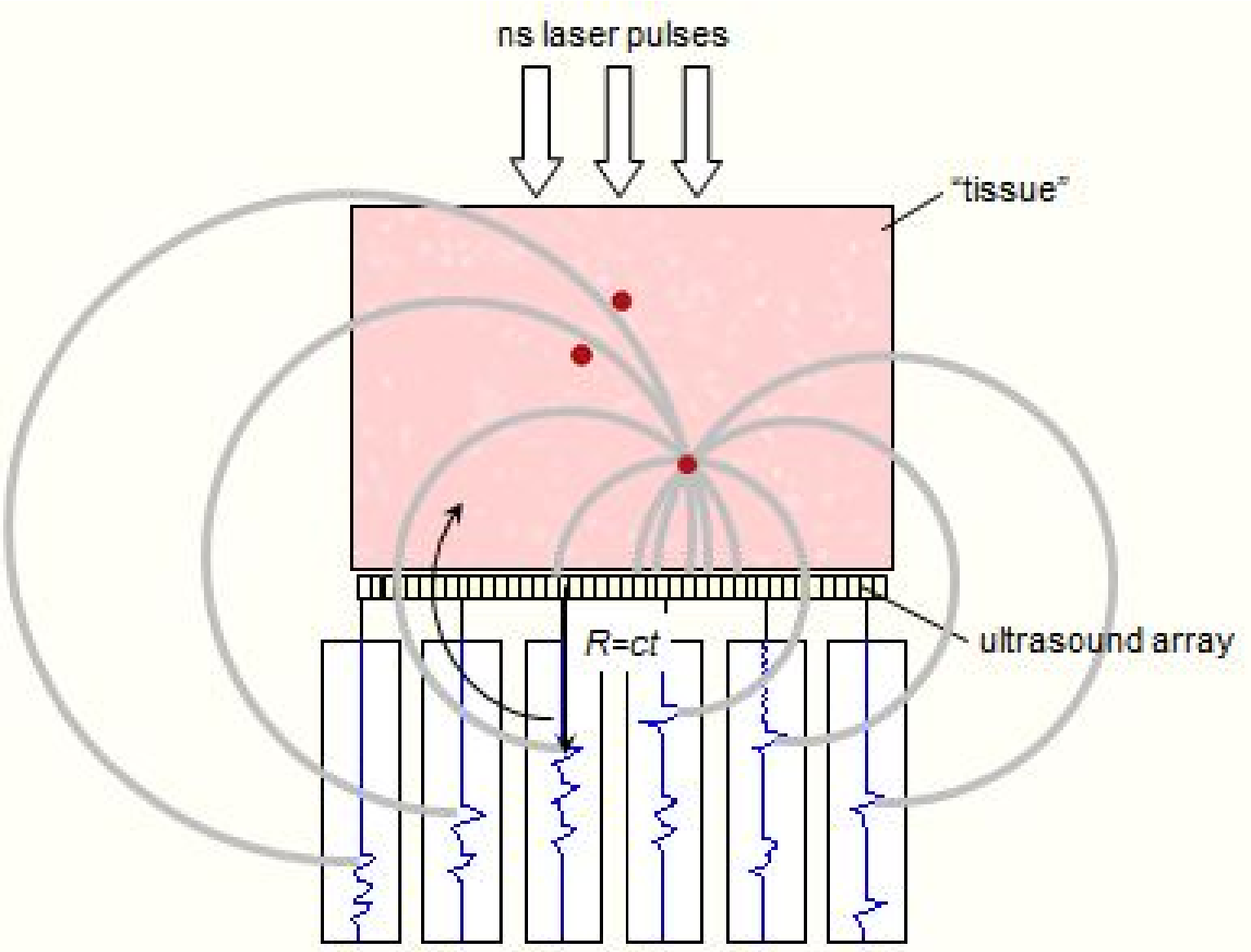

PhotoAcoustic Tomography

Some PAT systems

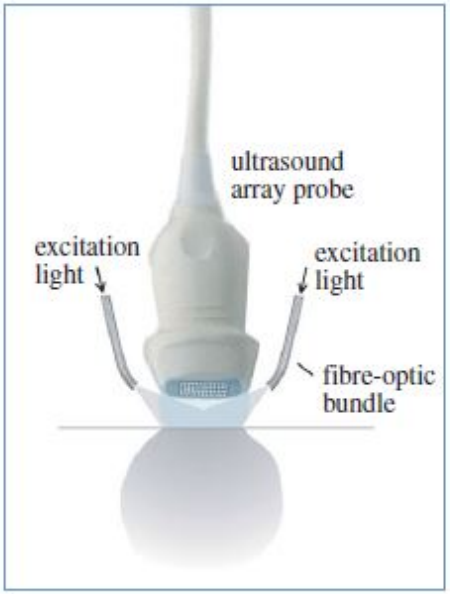

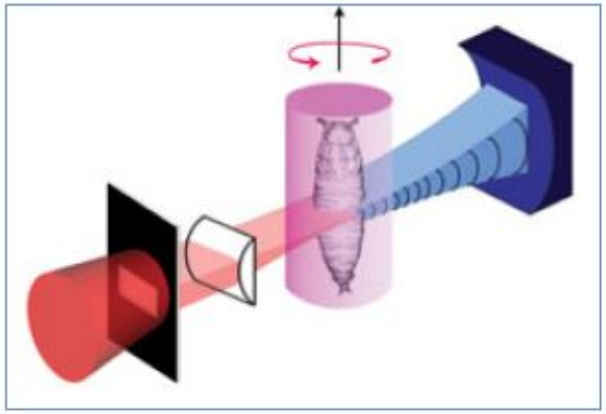

Razansky et al (2009) Nat. Phot. **3**, 412

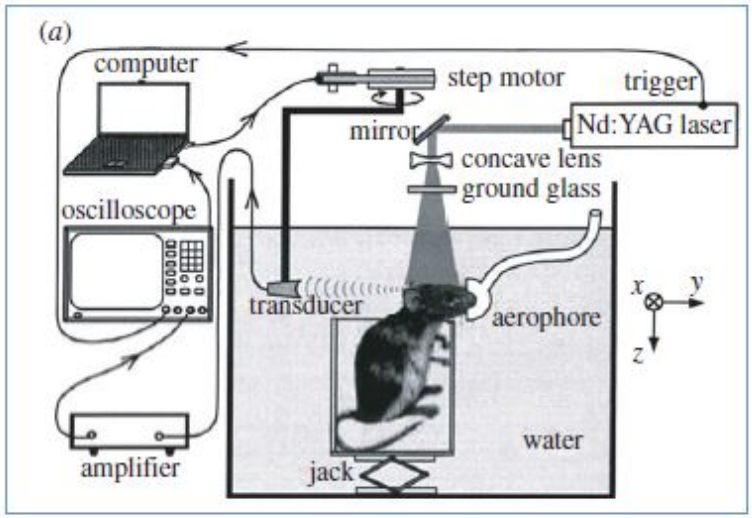

Wang et al. (2003) Nat. Biotech., **21**, 803 – 806.

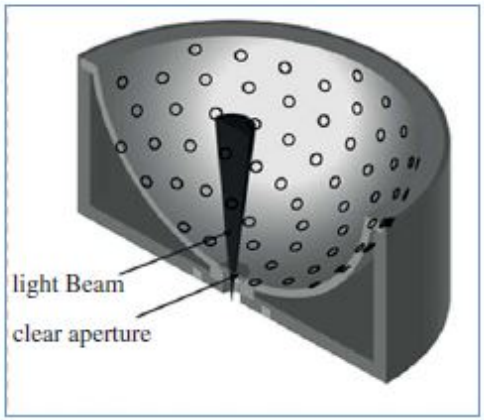

Kruger et al. (2010) Med. Phys. **37**, 6096

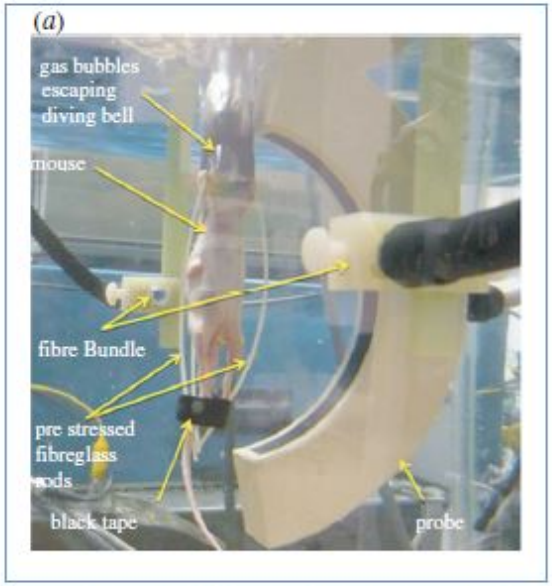

Brecht et al. (2009) JBO, **14**, 064007

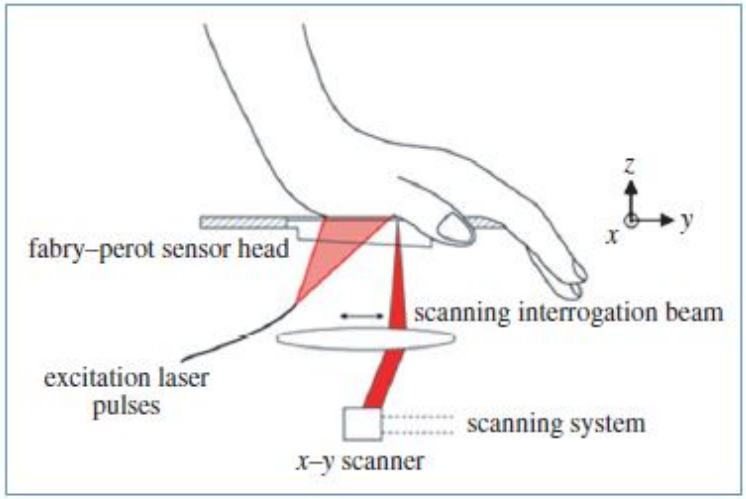

Zhang et al (2008) Appl. Opt., **47**, 561-577

Initial value Problem

$$\begin{aligned}\left(c^2(\boldsymbol{r})\nabla^2 - \frac{\partial^2}{\partial t^2}\right) p(\boldsymbol{r},t) &= 0 \qquad t \geq 0, \boldsymbol{r} \in \mathbb{R}^3 \\ p(\boldsymbol{r},0) &= \Gamma(\boldsymbol{r})\mu_a(\boldsymbol{r})\Phi(\boldsymbol{r}) \\ \left.\frac{\partial p(\boldsymbol{r},t)}{\partial t}\right|_{t=0} &= 0\end{aligned}$$

Data $p^{\text{obs}}(\boldsymbol{r}_s, t)$ measured on $\partial\Omega$, but model assumes propagation beyond this, i.e. $\partial\Omega$ is *not* a boundary condition
forward model

$$A : p_0(\boldsymbol{r}) \mapsto p^{\text{obs}}(\boldsymbol{r}_s, t) \qquad t \geq 0, \boldsymbol{r}_s \in \partial\Omega$$

In the constant speed case $c(\boldsymbol{r}) = c$, the signal detected at an observation point at time t is the sum of waves arriving from a distance $r = ct$.
This leads to the *Spherical Mean Transform* (SMT). In 3D this is stated

$$\mathcal{M}f(\boldsymbol{r}, t) := \frac{1}{4\pi} \int_{S^2} f(\boldsymbol{r} + ct\hat{\boldsymbol{s}}) \mathrm{d}^2 \hat{\boldsymbol{s}}$$

In analogy to the *Radon Transform* which integrates functions over planes, the SMT can be used as a basis for analytical inversions. In particular the adjoint of $\mathcal{M}$ can be used as the basis for *back Projection* and *Filtered Back Projection* formulae.

Filtered Back projection formulae for SMT (Finch, Patch, Rakesh, 2006), constant speed case. Complete data on sphere radius R. 'Universal' Backprojection, valid for spheres, cylinders and planes (Xu and Wang, 2005)

1. $$p_0(\boldsymbol{r}) = \frac{1}{8\pi^2}\nabla \cdot \int_{\partial\Omega} \hat{\mathbf{n}}(\boldsymbol{r}') \left(\frac{1}{\rho}\frac{\partial}{\partial\rho}\frac{p^{\text{obs}}(\boldsymbol{r}',\rho)}{\rho} \right)\Big|_{\rho=|\boldsymbol{r}'-\boldsymbol{r}|} \mathrm{d}^2\boldsymbol{r}'$$

2. $$p_0(\boldsymbol{r}) = -\frac{1}{8\pi^2}\int_{\partial\Omega} \frac{\partial}{\partial n} \left(\frac{1}{\rho}\frac{\partial}{\partial\rho}\frac{p^{\text{obs}}(\boldsymbol{r}',\rho)}{\rho} \right)\Big|_{\rho=|\boldsymbol{r}'-\boldsymbol{r}|} \mathrm{d}^2\boldsymbol{r}'$$

where $\hat{\mathbf{n}}(\boldsymbol{r}')$ is the outward normal vector to $\partial\Omega$. Differentiation in space is the filtering step, and integration over spheres is the backprojection step.
Extensions to arbitrary $n \geq 2$ in (Kunyansky 2007). More details (Kuchment 2014).

Initial value Problem

$$\begin{aligned}\left(c^2\nabla^2 - \frac{\partial^2}{\partial t^2}\right) p &= 0 \\ p|_{t=0} &= \Gamma \mu_a \Phi \\ \left.\frac{\partial p}{\partial t}\right|_{t=0} &= 0\end{aligned}$$

Initial value Problem

$$\begin{aligned}\left(c^2\nabla^2 - \frac{\partial^2}{\partial t^2}\right) p &= 0 \\ p|_{t=0} &= \Gamma \mu_a \Phi \\ \left.\frac{\partial p}{\partial t}\right|_{t=0} &= 0\end{aligned}$$

Boundary value Problem (t running backwards from T to 0)

$$\begin{aligned}\left(c^2\nabla^2 - \frac{\partial^2}{\partial t^2}\right) p &= 0 \\ p(\boldsymbol{r}, t)|_{t=T} &= 0 \\ p(\boldsymbol{r}, t)|_{\partial\Omega} &= p^{\text{obs}}(\boldsymbol{r}_s, t)\end{aligned}$$

Initial value Problem

$$\left(c^2\nabla^2 - \frac{\partial^2}{\partial t^2}\right) p = 0$$
$$p|_{t=0} = \Gamma \mu_a \Phi$$
$$\left.\frac{\partial p}{\partial t}\right|_{t=0} = 0$$

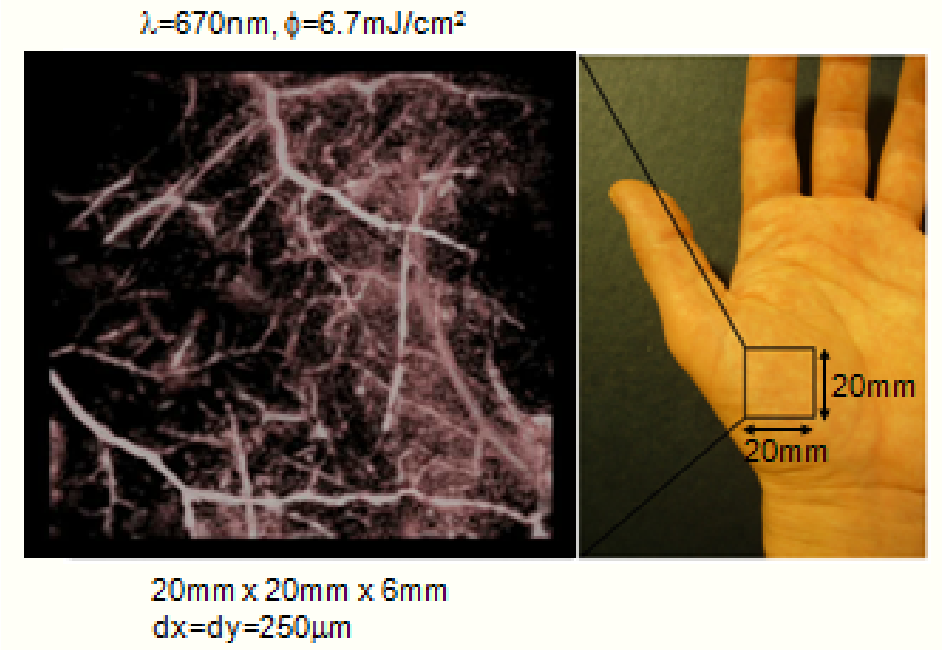

Boundary value Problem (t running backwards from T to 0)

$$\left(c^2\nabla^2 - \frac{\partial^2}{\partial t^2}\right) p = 0$$
$$p(\boldsymbol{r}, t)|_{t=T} = 0$$
$$p(\boldsymbol{r}, t)|_{\partial\Omega} = p^{\text{obs}}(\boldsymbol{r}_s, t)$$

Outline

1. Introduction
2. Modelling in Optical Tomography
3. PhotoAcoustics
4. Coupled Physics Imaging : Quantitative PhotoAcoustic Tomography
5. Summary
6. Acknowledgements

Coupled Physics Imaging

Quantitiative PhotoAcoustic Tomography

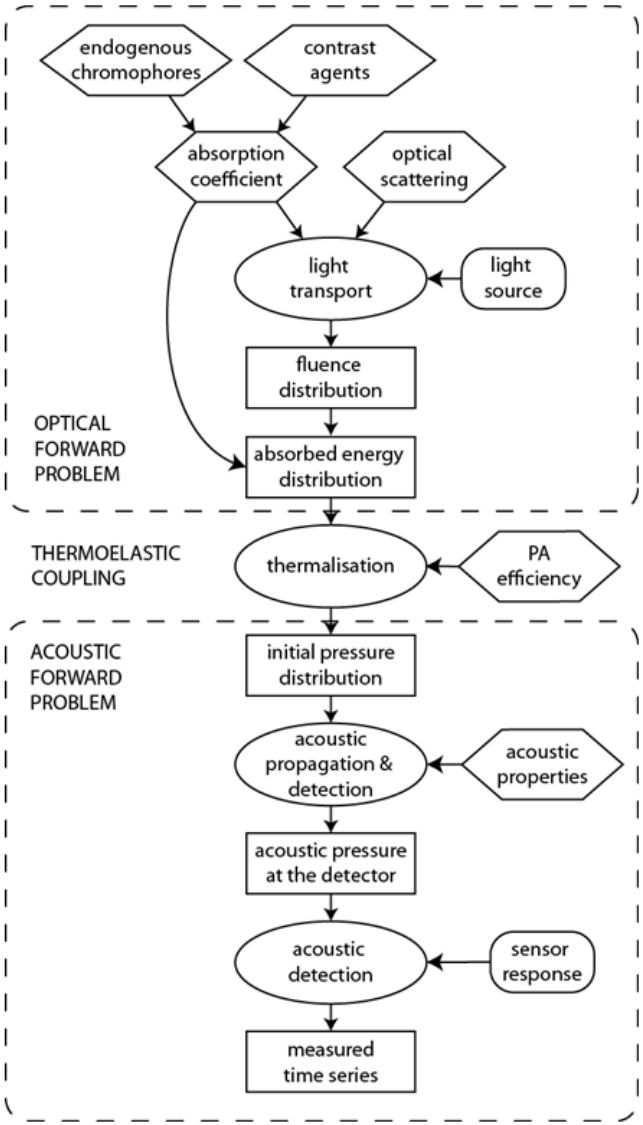

- Naturally occuring contrast agents (chromphores) give rise to optical absorption in the medium.
- The absorption and scattering coefficients μ_a and μ_s' determine the fluence distribution Φ,
- $\mu_a \Phi \mapsto H$ (deposited energy).
- $\Gamma H \mapsto p_0$ (pressure distribution) via thermalisation,
- p_0 propagates as an acoustic pulse (elasticity of tissue).
- Sensor detects PA time series $p(t)$.

Cox, A. Laufer, Beard, 2012.

Strategy used here : fit a model of light transport to the reconstructed data

$$\{\hat{\mu_a}, \hat{\mu_s}\} = \underset{\mu_a, \mu_s}{\arg\min} \left[\mathcal{E} := \frac{1}{2} ||H^{\text{obs}} - F(\mu_a, \mu_s)||^2 + R(\mu_a, \mu_s) \right]$$

where $F(\mu_a, \mu_s') = \mu_a \Phi(\mu_a, \mu_s')$ is the *forward model* of optical energy absorption, and R is a regularisation term.

- Forward model F can be based on RTE or diffusion.
- Principle regularisation term used : *Total Variation*.

Rearranging we get

$$D\mathcal{E}\begin{pmatrix}\mu_a^\delta\\ \mu_s^\delta\end{pmatrix} = -\left\langle \Phi(H^{\text{obs}} - F(\mu_a,\mu_s)), \mu_a^\delta\right\rangle_{L^2(\Omega)} + \left\langle \phi\phi^*, \mu_a^\delta\right\rangle_{L^2(\Omega\times S^{n-1})} + \left\langle \phi\phi^*, \mu_s^\delta\right\rangle_{L^2(\Omega\times S^{n-1})} - \left\langle \phi\mathcal{S}\phi^*, \mu_s^\delta\right\rangle_{L^2(\Omega\times S^{n-1})}$$

so that

$$\frac{\partial\mathcal{E}}{\partial\mu_a} = -\Phi(H^{\text{obs}} - F(\mu_a,\mu_s)) + \int_{S^{n-1}}\phi(\hat{\boldsymbol{s}})\phi^*(\hat{\boldsymbol{s}})\mathrm{d}\hat{\boldsymbol{s}}$$

$$\frac{\partial\mathcal{E}}{\partial\mu_s} = \int_{S^{n-1}}\phi(\hat{\boldsymbol{s}})\phi^*(\hat{\boldsymbol{s}})\mathrm{d}\hat{\boldsymbol{s}} - \int_{S^{n-1}}\int_{S^{n-1}}\phi(\hat{\boldsymbol{s}})\Theta(\hat{\boldsymbol{s}},\hat{\boldsymbol{s}}')\phi^*(\hat{\boldsymbol{s}}')\mathrm{d}\hat{\boldsymbol{s}}\mathrm{d}\hat{\boldsymbol{s}}'$$

Quantitative PhotoAcoustic Tomography

Matrix Free method

Explicit construction of Jacobians is too expensive $\Rightarrow$ use matrix free method based on adjoint fields

Limited memory BFGS optimisation

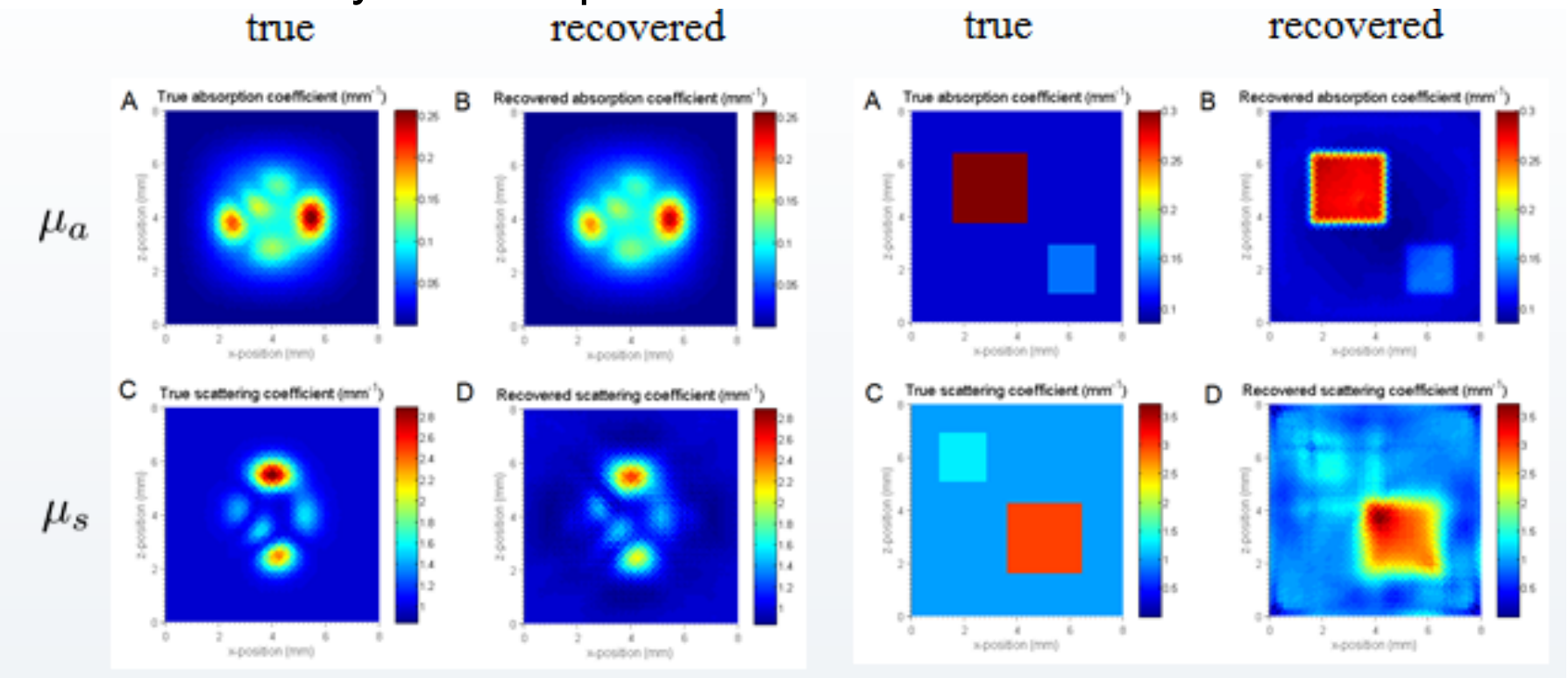

Using 4 images from 4 illumination directions, Tikhonov regularisation (Saratoon, Tarvainen, Cox, A., 2013)

Diffusion Approximation (DA) is solved with Finite Element Method (FEM). Discretisation :

$$\mu_{\mathrm{a}}(\boldsymbol{r}) \approx \mu_{\mathrm{a}}^{h}(\boldsymbol{r}) = \sum_{j=1}^{N_{\mathbf{a}}} \mu_{\mathrm{a},j} u_j(\boldsymbol{r}), \qquad \hat{\mu}_{\mathrm{a}} = (\mu_{\mathrm{a},1}, \ldots, \mu_{\mathrm{a},N_{\mathbf{a}}})$$

$$\mu'_{\mathrm{s}}(\boldsymbol{r}) \approx \mu_{\mathrm{s}}^{`h}(\boldsymbol{r}) = \sum_{j=1}^{N_{\mathbf{s}}} \mu'_{\mathrm{s},j} u_j(\boldsymbol{r}), \qquad \hat{\mu}'_{\mathrm{s}} = (\mu'_{\mathrm{s},1}, \ldots, \mu'_{\mathrm{s},N_{\mathbf{s}}})$$

$$\Phi(\boldsymbol{r}) \approx \Phi^{h}(\boldsymbol{r}) = \sum_{j=1}^{N_{\mathbf{F}}} \Phi_j u_j(\boldsymbol{r}), \qquad \hat{\Phi} = (\Phi_1, \ldots, \Phi_{N_{\mathbf{F}}})$$

FEM solution obtained by solving

$$K(x)\hat{\Phi}(x;q) = b(q) \Leftrightarrow \hat{\Phi}(x,q) = K^{-1}(x)b(q)$$

where K is the FEM matrix, b arises from the light source s, and $x = (\hat{\mu}_{\mathrm{a}}, \hat{\mu}'_{\mathrm{s}})$ is a vector of optical parameters.

The acoustic model is approximated with

$$\frac{1}{c^2}\frac{\partial}{\partial t^2}p(\boldsymbol{r},t) - \nabla^2 p(\boldsymbol{r},t) = \frac{1}{c^2}p_0(\boldsymbol{r})\frac{\partial}{\partial t}g_\tau(\boldsymbol{r},t)\,, \qquad \boldsymbol{r}\in\mathbb{R}^n, t\in\mathbb{R} \quad (11)$$

where g_τ is a Gaussian function approximating instantaneous heating (or delta function). Equation (11) has an analytical solution, that can be expressed as convolution

$$p(\boldsymbol{r},t) = \int_\Omega \frac{1}{c^2}p_0(\boldsymbol{r}')\mathcal{F}^{-1}\{\mathrm{i}\omega\hat{g}_\tau(\omega)\hat{G}(||\boldsymbol{r}-\boldsymbol{r}'||,\omega)\}(t)\mathrm{d}\boldsymbol{r}'$$

where $\mathcal{F}^{-1}\{\}(t)$ is the temporal inverse Fourier transform, $\hat{g}_\tau(\omega) = \mathcal{F}\{g_\tau(t)\}(\omega)$, and

$$\hat{G}(||\boldsymbol{r}-\boldsymbol{r}'||,\omega)\} = \begin{cases} \mathrm{i}\frac{1}{4}H_0^{(1)}\left(\frac{w}{c}||\boldsymbol{r}-\boldsymbol{r}'||\right), & n=2 \\ \frac{1}{4\pi||\boldsymbol{r}-\boldsymbol{r}'||}\exp\left(\mathrm{i}\frac{w}{c}||\boldsymbol{r}-\boldsymbol{r}'||\right) & n=3 \end{cases}$$

is the Green's function defined by $\nabla^2\hat{G} + \frac{\omega^2}{c^2}\hat{G} = -\delta(\boldsymbol{r})$.

Approximating p_0 with base functions v_m as

$$p_0(\boldsymbol{r}) \approx p_0^h(\boldsymbol{r}) = \sum_{m=1}^{M} p_{0,m} v_m(\boldsymbol{r}) \quad \hat{p}_0 = (p_{0,1}, \ldots, p_{0,M})$$

the photoacoustic time series at detector located at $d_k (k = 1 \ldots n_K)$ is

$$p(d_k, t) = \sum_{m=1}^{M} p_{0,m} w_m(d_k, t)$$

where

$$w_m(\boldsymbol{r}, t) = \int_\Omega \frac{1}{c^2} v_m(\boldsymbol{r}') \mathcal{F}^{-1} \left\{ \mathrm{i}\omega \hat{g}_\tau(\omega) \hat{G}(||\boldsymbol{r} - \boldsymbol{r}'||, \omega) \right\} (t) \mathrm{d}\boldsymbol{r}' \qquad (12)$$

$$\hat{p}_t = \mathbf{W} \hat{p}_0$$

with $\mathbf{W}$ being formed by e.g. Gaussian quadrature integration of (12).

By writing

$$p_{0,q} = \gamma \mu_{\mathrm{a},q} \Phi_q$$

and assuming γ being known, the combined photoacoustic model describing acoustic time series corresponding to optical parameters $x = (\hat{\mu}_{\mathrm{a}}, \hat{\mu}'_{\mathrm{s}})$ and illumination q is then

$$\hat{p}_t = \mathbf{W} \mathrm{diag}\left\{\hat{\mu}_{\mathrm{a}}\right\} K^{-1}(x) b(q).$$

By writing

$$p_{0,q} = \gamma \mu_{a,q} \Phi_q$$

and assuming γ being known, the combined photoacoustic model describing acoustic time series corresponding to optical parameters $x = (\hat{\mu}_a, \hat{\mu}'_s)$ and illumination q is then

$$\hat{p}_t = \mathbf{W} \text{diag}\left\{\hat{\mu}_a\right\} K^{-1}(x) b(q).$$

Given n_Q illuminations $q_1 \ldots q_{n_Q}$, and corresponding photoacoustic time series $\hat{p}_{t;1}, \ldots, \hat{p}_{t,n_Q}$, the forward model can be written as

$$z = f(x),$$

with

$$z = \left(\hat{p}_{t;1}, \ldots, \hat{p}_{t,n_Q}\right) \in \mathbb{R}^{n_K \times n_T \times n_Q}$$

and $f(x) : \mathbb{R}^{N_a+N_s} \rightarrow \mathbb{R}^{n_K \times n_T \times n_Q}$ given by

$$f(x) = \left(\mathbf{W} \text{diag}\left\{\hat{\mu}_a\right\} K^{-1}(x) b(q_1), \ldots, \mathbf{W} \text{diag}\left\{\hat{\mu}_a\right\} K^{-1}(x) b(q_{n_Q})\right)$$

Inverse Problem

Bayesian Approach

Taking Bayesian approach to the photoacoustic inverse problem, and assuming additive noise model

$$y = f(x) + e$$

where y is $z = f(x)$ polluted by noise e,

Inverse Problem

Bayesian Approach

Taking Bayesian approach to the photoacoustic inverse problem, and assuming additive noise model

$$y = f(x) + e$$

where y is $z = f(x)$ polluted by noise e, the posterior distribution, corresponding to additive noise model, is

$$\pi(x|y) \propto \pi_x(x)\pi_e(y - f(x)),$$

where π_e and π_x are the probability densities of the noise and the prior.

Inverse Problem

Bayesian Approach

Taking Bayesian approach to the photoacoustic inverse problem, and assuming additive noise model

$$y = f(x) + e$$

where y is $z = f(x)$ polluted by noise e, the posterior distribution, corresponding to additive noise model, is

$$\pi(x|y) \propto \pi_x(x)\pi_e(y - f(x)),$$

where π_e and π_x are the probability densities of the noise and the prior.

Assuming Gaussian distribution for the noise e and the prior of x

$$e \sim \mathcal{N}(\eta_e, \Gamma_e), \quad x \sim \mathcal{N}(\eta_x, \Gamma_x)$$

the *maximum a posteriori* (MAP) estimate can be obtained as

$$x_{\text{MAP}} = \arg\min_x \left[||L_e(y - f(x) - \eta_e)||^2 + ||L_x(x - \eta_x)||^2 \right],$$

where $L_e L_e^{\mathrm{T}} = \Gamma_e^{-1}$ and $L_x L_x^{\mathrm{T}} = \Gamma_x^{-1}$ are Cholesky decompositions of the covariance matrices.

Inverse Problem

Bayesian Approach - continued

In addition to point estimates, such as MAP, Bayesian approach enables approximation of the error of the estimate. One such approximation is the credibility interval.

Inverse Problem

Bayesian Approach - continued

In addition to point estimates, such as MAP, Bayesian approach enables approximation of the error of the estimate. One such approximation is the credibility interval.
Given MAP estimate x_{MAP}, it is possible to linearize the forward model $f(x)$ using Taylor series as

$$f(x) \approx f(x_{\mathrm{MAP}}) + \mathbf{J}_{f(x_{\mathrm{MAP}})}(x - x_{\mathrm{MAP}});$$

where $\mathbf{J}_{f(x_{\mathrm{MAP}})}$ is the Jacobian of f evaluated at x_{MAP}.

Inverse Problem

Bayesian Approach - continued

In addition to point estimates, such as MAP, Bayesian approach enables approximation of the error of the estimate. One such approximation is the credibility interval.
Given MAP estimate x_{MAP}, it is possible to linearize the forward model $f(x)$ using Taylor series as

$$f(x) \approx f(x_{\mathrm{MAP}}) + \mathbf{J}_{f(x_{\mathrm{MAP}})}(x - x_{\mathrm{MAP}});$$

where $\mathbf{J}_{f(x_{\mathrm{MAP}})}$ is the Jacobian of f evaluated at x_{MAP}. Substituting the linearization into the observation model

$$y = f(x_{\mathrm{MAP}}) + \mathbf{J}_{f(x_{\mathrm{MAP}})}(x - x_{\mathrm{MAP}}) + e,$$

one finds posterior distribution being approximated as Gaussian, s.t.

$$x|y \propto \mathcal{N}(\eta, \Gamma),$$

where $\eta = x_{\mathrm{MAP}}$, and $\Gamma = \left(\mathbf{J}_f^{\mathrm{T}} \Gamma_e^{-1} \mathbf{J}_f + \Gamma_x^{-1}\right)^{-1}$

is the approximative covariance matrix of the posterior distribution of the original inverse problem.

The approximative credibility interval is then

$$C_\alpha = [x_{\mathrm{MAP}} - \alpha\sigma, x_{\mathrm{MAP}} + \alpha\sigma];$$

where σ is vector of square roots of the diagonals of Γ, and α is 1, 2, or 3 for 68.3%, 95.5%, and 99.7% credibility intervals respectively.

The approximative credibility interval is then

$$C_\alpha = [x_{\mathrm{MAP}} - \alpha\sigma, x_{\mathrm{MAP}} + \alpha\sigma];$$

where σ is vector of square roots of the diagonals of Γ, and α is 1, 2, or 3 for 68.3%, 95.5%, and 99.7% credibility intervals respectively.
It must be emphasized, that the credibility interval is dependent on the forward model and the prior. If either the model or the prior information is poor, then the estimates (and the credibility intervals) are bound to be misleading.

Simulations

The investigated domain was $[-5mm, 5mm]^n$, $n = 2$ and $n = 3$.
μ_a varied between $0.07 - 0.98 mm^{-1}$ and μ_s' between $0.75 - 1.36 mm^{-1}$. Sound speed of c = 1500 m=s was used.
The data was formed by two different illuminations. Each illumination had light entering the investigated domain from 1-3 sides with both illluminations covering at least 2 sides.
Acoustic detectors were located densely on 1-4 sides (2D) and 1 side (3D) of the domain, as well as sparsely on a circle (2D). Number of detectors was 31 - 128 (2D) and 1089 (3D).
Measurement data was simulated in grid with $37^2 = 1369$ (2D) and 373 = 50653 (3D) nodes. Reconstructions were computed in grids with 312 = 961 (2D) and 313 = 29791 (3D) nodes.
Noise was added to the simulated photoacoustic time series with standard deviation being 5%, 1%, or 0.1% of the peak-to-peak pressure amplitude.

Simulations (continued)

Accurate noise statistics were assumed in the reconstructions. Ornstein-Ohlenbeck was used for the prior with $\zeta = 1mm$. Prior parameters were chosen for μ_a and μ_s' separately, s.t. the mean of the prior corresponded to mean of peak-to-peak variation of parameters, and peak-to-peak variation corresponed to mean $\pm$ standard deviation of the prior:

$$\eta = \frac{1}{2}(\text{max+min}), \quad \sigma = \frac{1}{2}(\text{max- min}),$$

MAP estimates were obtained in 2D and 3D for varying illumination and acoustic detector setups. 99.7% credibility intervals were computed for some 2D estimates.

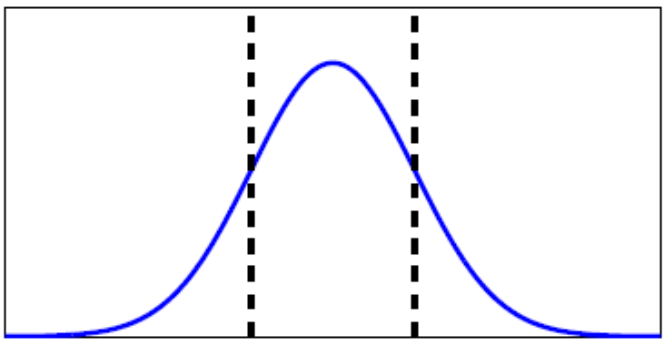

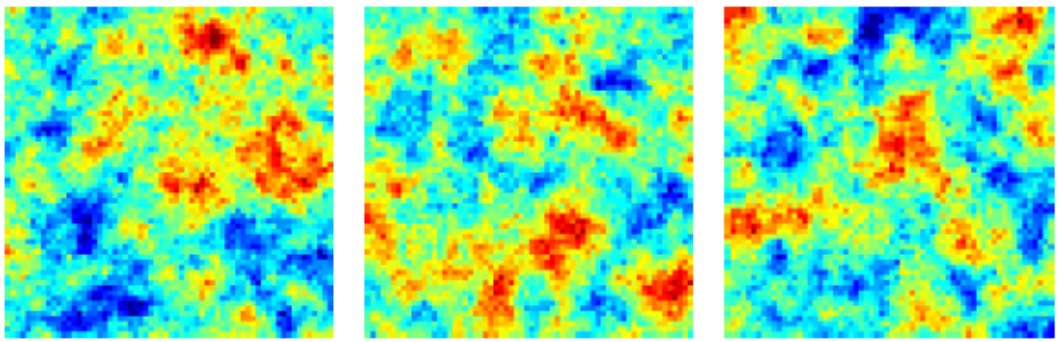

Simulations (2D)

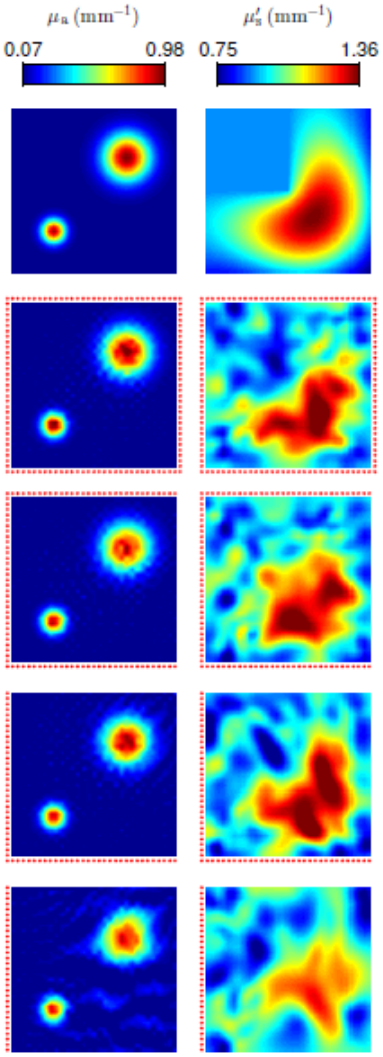

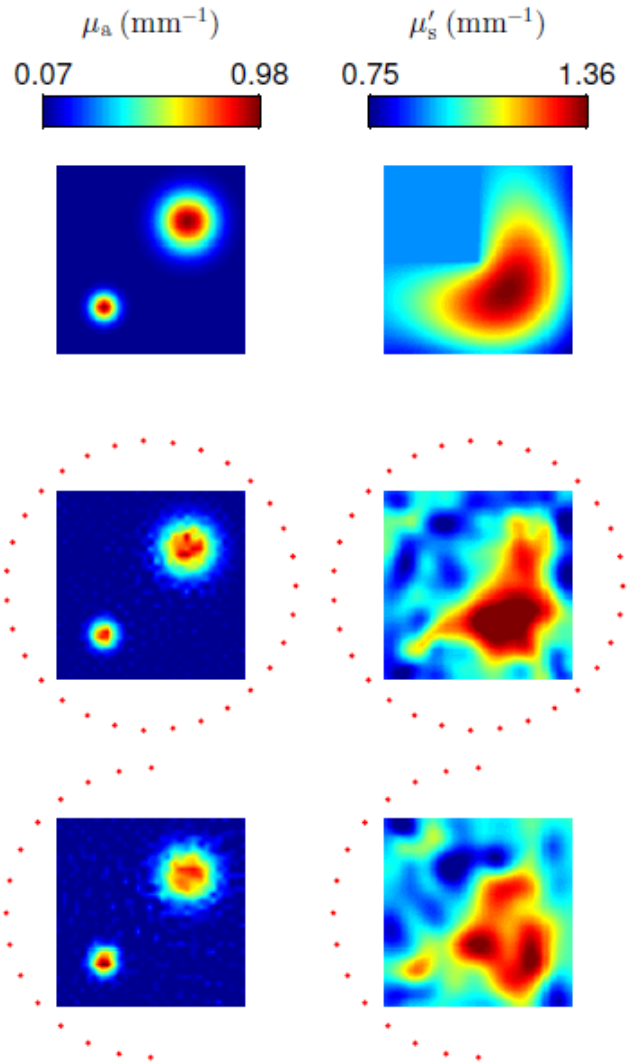

Reconstructions for different acoustic detector configurations. Illuminations from $\Leftarrow + \Rightarrow$ and $\Uparrow + \Downarrow$. Noise level 1%.

Simulations (2D)

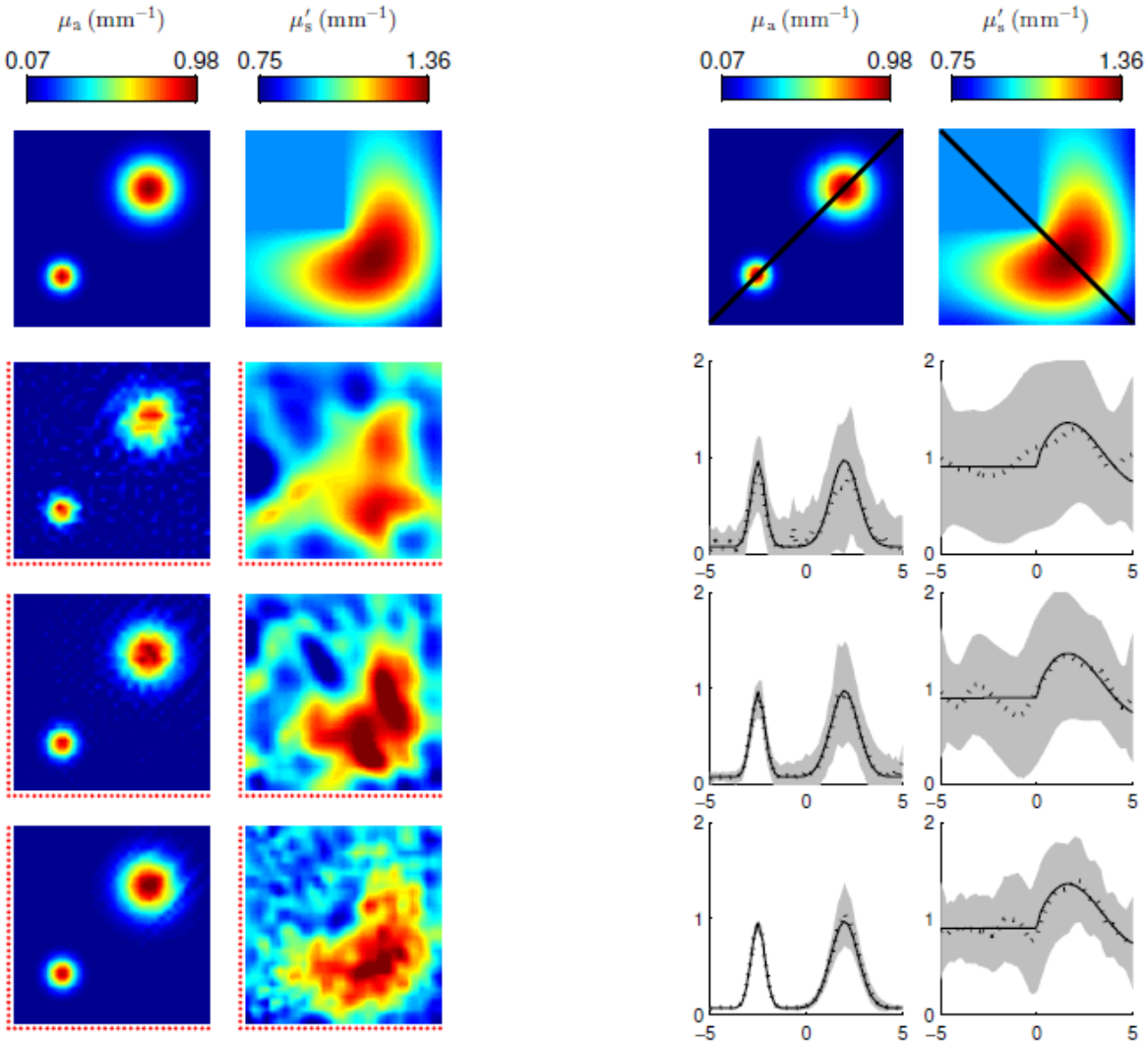

Reconstructions and 99.7% credibility intervals for 5%, 1%, and 0.1% noise. Illuminations from $\Leftarrow + \Rightarrow$ and $\Uparrow + \Downarrow$.

Simulations (2D)

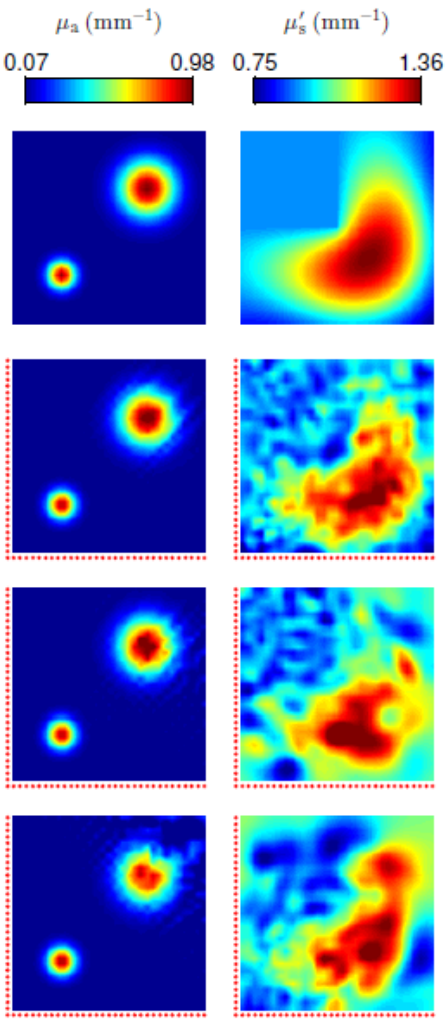

Reconstructions for different illuminations. 0.1% noise. Illuminations are 1) $\Leftarrow + \Rightarrow$ and $\Uparrow + \Downarrow$, 2) $\Leftarrow + \Downarrow$ and $\Uparrow$, 3) $\Leftarrow$ and $\Downarrow$.

Simulations (3D)

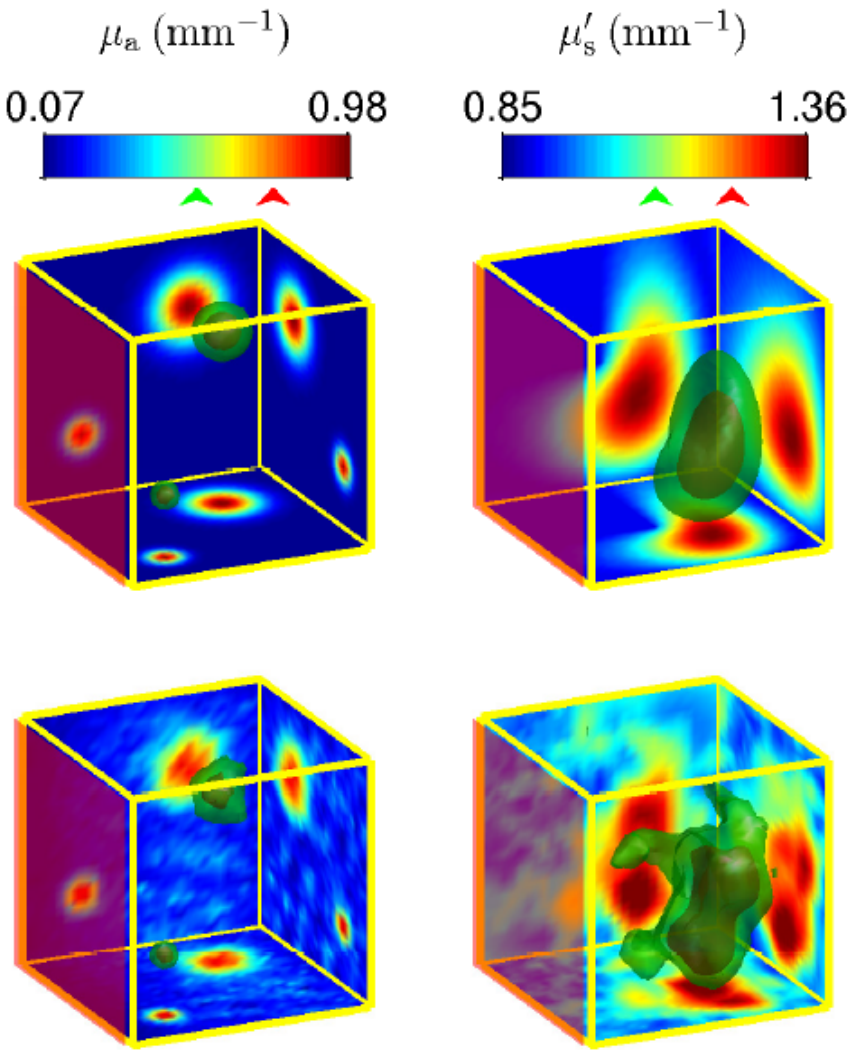

Reconstructions in 3D. Illuminations from three front sides and three back sides. Noise 0.1%. Acoustic detectors on the red edge.

Outline

1. Introduction
2. Modelling in Optical Tomography
3. PhotoAcoustics
4. Coupled Physics Imaging : Quantitative PhotoAcoustic Tomography
5. Summary
6. Acknowledgements

Summary

1. Optical Tomography is of interest because of its spectral contrast that relate to functional activity of tissues
   - Low resolution but relatively fast
   - Inverse problems in parameter identification, source identification, or both
   - Multimodality systems provide complementary information

Summary

1. Optical Tomography is of interest because of its spectral contrast that relate to functional activity of tissues
   - Low resolution but relatively fast
   - Inverse problems in parameter identification, source identification, or both
   - Multimodality systems provide complementary information
2. Photoacoustic imaging : seeing optical contrast with high resolution
   - an example of “Coupled Physics Imaging”, not just data fusion
   - large variety of systems with different resolution/speed/depth penetration trade off

Summary

1. Optical Tomography is of interest because of its spectral contrast that relate to functional activity of tissues
   - Low resolution but relatively fast
   - Inverse problems in parameter identification, source identification, or both
   - Multimodality systems provide complementary information
2. Photoacoustic imaging : seeing optical contrast with high resolution
   - an example of “Coupled Physics Imaging”, not just data fusion
   - large variety of systems with different resolution/speed/depth penetration trade off

Many challenges remain, in solving both the acoustic and optical inverse problems together : “Quantitative PhotoAcoustic Tomography”.

Summary

1. Optical Tomography is of interest because of its spectral contrast that relate to functional activity of tissues
   - Low resolution but relatively fast
   - Inverse problems in parameter identification, source identification, or both
   - Multimodality systems provide complementary information
2. Photoacoustic imaging : seeing optical contrast with high resolution
   - an example of “Coupled Physics Imaging”, not just data fusion
   - large variety of systems with different resolution/speed/depth penetration trade off

Many challenges remain, in solving both the acoustic and optical inverse problems together : “Quantitative PhotoAcoustic Tomography”. Next step : combine numerical methods (time -reversal) with optical models (radiative transport equation).

Summary

1. Optical Tomography is of interest because of its spectral contrast that relate to functional activity of tissues
   - Low resolution but relatively fast
   - Inverse problems in parameter identification, source identification, or both
   - Multimodality systems provide complementary information
2. Photoacoustic imaging : seeing optical contrast with high resolution
   - an example of “Coupled Physics Imaging”, not just data fusion
   - large variety of systems with different resolution/speed/depth penetration trade off

Many challenges remain, in solving both the acoustic and optical inverse problems together : “Quantitative PhotoAcoustic Tomography”.
Next step : combine numerical methods (time -reversal) with optical models (radiative transport equation).
The goal is to get high resolution, dynamic and spectrally resolved quantitiative images (5D).

Outline

1. Introduction
2. Modelling in Optical Tomography
3. PhotoAcoustics
4. Coupled Physics Imaging : Quantitative PhotoAcoustic Tomography
5. Summary
6. Acknowledgements

Acknowledgements

- **Collaborators :**
  - *UCL*: P.Beard, M.Betcke, T.Betcke, T.Correia, B.Cox, J. Hebden, A. Gibson, J. Heiskala, E.Hillman, S.Prince, T.Saratoon, M.Schweiger, V. Soloviev, A.Zacharopoulos
  - *Imperial*: P.French, J. McGinty,
  - *Manchester* O.Dorn, B.Lionheart
  - *Kuopio*: J. Kaipio, V. Kolehmainan, T. Tarvainen, M. Vaukhonen,
  - *Helsinki*: J. Heino, P. Hiltunen, I.Nisilla, S. Siltanen, E. Somersalo,
  - *Milan*: A. Bassi, R. Cubeddu, C. D'Andrea, G. Valentini
  - *Heraklion*: J. Ripoll
  - *MGH*: D. Boas
  - *UPenn*: R. Choe, A. Yodh
- **Funding**
  - This work was supported by EPSRC grant EP/E034950/1 and by the Academy of Finland (projects 122499, 119270 and 213476)
  - *Other funding* : MRC, Wellcome Trust, CEC Framework, Royal Society